UNIVERSITY OF LEEDS

This is a repository copy of *Highly Tough Hydrogels with the Body Temperature-Responsive Shape Memory Effect*.

White Rose Research Online URL for this paper:
http://eprints.whiterose.ac.uk/154012/

Version: Accepted Version

Article:
Liang, R, Yu, H, Wang, L et al. (3 more authors) (2019) Highly Tough Hydrogels with the Body Temperature-Responsive Shape Memory Effect. ACS Applied Materials & Interfaces, 11 (46). pp. 43563-43572. ISSN 1944-8244

https://doi.org/10.1021/acsami.9b14756

© 2019 American Chemical Society. This document is the Accepted Manuscript version of a Published Work that appeared in final form in ACS Applied Materials and Interfaces, copyright © American Chemical Society after peer review and technical editing by the publisher. To access the final edited and published work see https://doi.org/10.1021/acsami.9b14756

Reuse
Items deposited in White Rose Research Online are protected by copyright, with all rights reserved unless indicated otherwise. They may be downloaded and/or printed for private study, or other acts as permitted by national copyright laws. The publisher or other rights holders may allow further reproduction and re-use of the full text version. This is indicated by the licence information on the White Rose Research Online record for the item.

Takedown
If you consider content in White Rose Research Online to be in breach of UK law, please notify us by emailing eprints@whiterose.ac.uk including the URL of the record and the reason for the withdrawal request.

White Rose university consortium
Universities of Leeds, Sheffield & York

eprints@whiterose.ac.uk
https://eprints.whiterose.ac.uk/

Highly Tough Hydrogels with Body Temperature-Responsive Shape Memory Effect

Ruixue Liang[†], *Haojie Yu*[†,*], *Li Wang*[†,*], *Long Lin*[‡], *Nan Wang*[†], *Kaleem-ur-Rahman Naveed*[†]

[†]State Key Laboratory of Chemical Engineering, Institute of Polymer and Polymerization Engineering, College of Chemical and Biological Engineering, Zhejiang University, Hangzhou 310027, China

[‡]Department of Colour Science, University of Leeds, Woodhouse Lane, Leeds LS2 9JT,

KEYWORDS: hydrogen bonds, hydrophobic interactions, hydrogel, shape memory effect, body temperature responsiveness, high mechanical performance.

ABSTRACT: Shape memory hydrogels, a promising class of smart materials for biomedical applications, have attracted increasing research attention owing to their tissue-like water-rich network structure. However, preparing shape memory hydrogels with high mechanical strength and body temperature-responsiveness has proven to be an extreme challenge. This study presents a facile and scalable methodology to prepare highly tough hydrogels with body temperature-responsive shape memory effect based on synergetic hydrophobic interactions and hydrogen bonding. 2-phenoxyethyl acrylate (PEA) and acrylamide (AAm) were chosen as hydrophobic monomer and hydrophilic hydrogen bonding monomer, respectively. The prepared hydrogels exhibited a maximum tensile strength of 5.1±0.16 MPa with satisfactory stretchability, and the mechanical strength showed a strong dependence on temperature. Besides, the hydrogel with 60 mol% PEA shows an excellent body temperature-responsive shape memory behavior with almost 100% shape fixity and shape recovery. Furthermore, we applied the hydrogels as shape memory embolization plug for simulating vascular occlusion, and the embolism performance was preliminarily explored in vitro.

MAIN TEXT

1. INTRODUCTION

As an emerging category of smart materials, shape memory hydrogels (SMHs) are capable of being fixed in one or more programmed temporary shape(s) and recovering to the permanent shape upon exposure to suitable stimuli. [1-2] SMHs have attracted increasing research interest during the recent decade. [3] In comparison with the conventional hydrophobic shape memory polymers, the water-rich

environment endows SMHs with soft and wet characters [4], affording them great potential application in areas such as drug delivery matrices, [5] tissue engineering scaffolds, [6] soft actuators, [7] biomedical materials, [3] and so on. To date, technologies such as supramolecular chemistry [7-10] and double network construction[11-13] have greatly facilitated the development of SMHs, and as a result, various hydrogels having shape memory capability in response to stimuli including pH, temperature, light and chemicals have been fabricated in recent years. Among these types of SMHs, the thermo-responsive ones have been investigated in depth and have played a predominant role because of their outstanding response rate (as quick as several seconds), shape fixity ratio (R_f) and shape recovery ratio (R_r), all of which are attractive properties for application. [14-16]

SMHs have played a vital role in biomedical applications [3, 17] (e.g. applied in human body as implantable materials [18]) because of their 3D structure and tissue-like aqueous environment. [19] Generally, thermo-responsive SMHs employed as biomedical materials have to meet at least two essential requirements: a suitable trigger temperature [20] and a strong mechanical strength [21]. On one hand, excessive trigger temperature is not suitable for in vivo applications since temperature greater than 50 °C may cause irreversible damage to tissue, [20, 22] and low mechanical strength limits the load-bearing performance. [21] On the other hand, thermo-responsive SMHs with a trigger temperature above 37 °C are difficult to be self-actuated by body heat, necessitating an extrinsic heating source, which would lead to complex application procedure and likely overheating that may also cause tissue damage. [20] Thus, thermo-responsive SMHs having a trigger temperature lower than, but close to, 37 °C is more compliant for biomedical applications. [22] However, fabrication of thermo-responsive

SMHs that operate at this ideal trigger temperature, as well as having a considerable mechanical strength remains a challenge.

Researchers have devoted much effort to developing tough hydrogels with thermo-responsive shape memory effect (SME), but very few of such hydrogels developed so far can be activated at body temperature. [23-26] By introducing temperature-sensitive physical interactions such as hydrophobic interaction [26], crystalline domain [23], hydrogen bonding [7, 25] or π-π stacking [27] into hydrophilic hydrogel network, thermo-responsive SMHs with great mechanical strength can be obtained. These physical interactions not only bestow hydrogel networks with remarkable energy dissipation capability due to their dynamic and reversible nature, but also function as molecular switches to fix or release programmed temporary shapes in response to heat.[1, 28] However, the trigger temperature of SMHs based on this approach is usually dependent on the dissociation temperature of the physical interactions, making it difficult to adjust the trigger temperature to body temperature.[14, 23, 26-27, 29] For example, the preparation of temperature-responsive SMHs by introducing hydrophobic 2-(N-ethylperfluoro-octanesulfonamido) ethyl methacrylate (FOSM) into hydrophilic network were reported.[26] The fluorocarbon hydrophobes of FOSM form strong hydrophobic interactions in aqueous medium, serving as temperature-sensitive physical crosslinks to endow the hydrogel with considerable mechanical strength and temperature-responsive shape memory capability. However, the trigger temperature was mainly determined by the glass transition temperature of the hydrophobic nanodomains (about 45 °C). Similarly, adjusting trigger temperature of semi-crystalline hydrogel networks, i.e. melting temperature (T_m) is also difficult [23]. Although construction of dual-physical crosslinkings consisting of hydrogen bonds and dipole-dipole interactions [16, 30] or grafting of

crystallisable side chain with T_m slightly lower than 37 °C (e.g. oligotetrahydrofuran [31]) has proved to be feasible strategies, drawbacks including the requirement of specific monomers or low mechanical strength limit their application.

In this paper, a strategy based on synergistic hydrophobic interactions and hydrogen bonds was developed to prepare body temperature-responsive SMHs with strong mechanical strength. Commercially available 2-phenoxyethyl acrylate (PEA) and acrylamide (AAm) were chosen as hydrophobic monomer and hydrogen bonding monomer, respectively. The poly(PEA-co-AAm) hydrogels were prepared by random copolymerizations (Figure 1 A) and via a previously reported solvent exchange method (Figure 1B)[16, 27]. Firstly, PEA, AAm and chemical crosslinker PEGDA700 were dissolved in DMSO, and the as-prepared organogels were fabricated after thermal initiation in a self-made mould. Secondly, complete replacement of the absorbed DMSO by deionized (DI) water resulted in the conversion from organogels to hydrogels. The synergistic dual-physical crosslinks endow the hydrogels with a high mechanical strength which is strongly sensitive to body temperature. Compared to previous works, the fabrication method is facile and, to some degree, universal. This work provides a new idea for researchers to obtain robust SMHs with body temperature responsiveness, which may be a technology-push to SMHs in broadening the applications.

2. EXPERIMENTAL SECTION

2.1 Materials

2-phenoxyethyl acrylate (PEA 90%), 2-phenoxyethyl methacrylate (PEMA, 85%), acrylamide (AAm, 99%), N, N-dimethylacrylamide (DMAA, 99%), 2, 2'-azobis(2, 4-dimethylvaleronitrile) (ABVN, 97%) were purchased from J&K Scientific Ltd. Benzyl acrylate (BzA, 97%), was purchased from Aladdin Reagent Co., Ltd. Poly(ethylene glycol) diacrylate (PEGDA-700, Mn=700) was purchased from Macklin Biochemical Co., Ltd. Dimethyl sulphoxide （DMSO, 99%） was purchased from Sinopharm Chemical Regent Co. Ltd. ABVN was recrystallized before used. All the other chemicals were used as received unless otherwise stated.

2.2 Preparation of hydrogels

Poly(PEA-co-AAm) hydrogels were prepared by random co-polymerization of AAm, PEA and PEGDA-700 using DMSO as solvent. In the reaction system, the concentration of the precursor polymer solutions was fixed at 4M, and only the mole fraction of PEA (R_{PEA}) relative to the total monomer amount was the control parameter. Hereafter, the poly(PEA-co-AAm) hydrogel samples are denoted as Px-Ay, where x and y are the mole percentage of PEA and AAm relative to the total monomer amount. Typically, to prepare the hydrogel P60-A40, 7391.0 mg (38.5 mmol) PEA, 1814.7 mg (25.5 mmol) AAm and 23.0 mg (0.033 mmol) PEGDA-700 were dissolved in 7.7 ml DMSO to form a 4M monomer solution. The solution was subsequently degassed with argon for 0.5 h to remove the dissolved O_2. Thereafter, 31.6 mg (0.13 mmol) initiator ABVN was added to the solution and stirred for 1 min. The resultant solution was injected into a mould (disk mould which was composed of two pieces of glass sheets with a silicon rubber spacer, 80mm×80mm×1.2mm; Teflon tube with an inner diameter of 3.0 mm) under argon atmosphere. The reaction was allowed to last for 10 h at 50 ^{o}C to obtain an as-prepared organogel. Subsequently, the P60-A40 hydrogel was obtained

by immersing the organogel into deionized (DI) water for 2 weeks to remove the DMSO completely. Poly(PEA-co-DMAA), poly(PEMA-co-AAm) and poly(BzA-co-AAm) hydrogels were prepared using the same method as that of poly (PEA-co-AAm). The fundamental recipes for preparing the hydrogels are shown in Table S1 and S2.

2.3 Characterization

Determination of equilibrium water contents (EWCs)

EWCs were determined gravimetrically. Firstly, the hydrogel samples were fully swollen in DI water and then dried under vacuum at 40 ^{o}C until constant weight. The EWC was calculated by the equation:

$$EWC = \frac{m_1 - m_0}{m_1} \times 100\%$$

Where m_1 and m_0 are the weights of the swollen hydrogels and the completely dried hydrogels, respectively.

Mechanical performance test

Organogels were tested at the as-prepared state, while all the hydrogels were tested after being swollen in equilibrium at room temperature. All the samples were cut into uniform dumbbell-shaped specimens (width: 2 mm; gauge length: 20 mm, thickness: 1 mm) and coated with silicone grease to limit the volatilization of water or DMSO. All the tests were performed on a universal testing machine (Zwick/Roell Z020, Germany) with a 500 N load cell. At least five parallel samples were

recorded for each sample. For the tensile strength study, all the tests were conducted under a constant crosshead speed of 100 mm/min at 22 ^{o}C. For the study on temperature-dependent mechanical behavior, the tests were conducted under a constant crosshead speed of 100 mm/min at different temperatures of 16, 20, 24 and 37 ^{o}C. For the study on deformation-rate dependence of mechanical behavior, the tests were conducted under different crosshead speeds of 10, 100, 200, 500 mm/min at 22 ^{o}C. For the loading-unloading test, all the samples were subjected to a strain of 200% under constant crosshead speed of 100 mm/min at 22 ^{o}C. The dissipated energy (ΔU) during the loading-unloading cycle, which was determined by the area of the hysteresis loop, was calculated by using the following equation[32]:

$$\Delta U = \int_{loading} \sigma d\varepsilon - \int_{unloading} \sigma d\varepsilon$$

Where σ and ε *are refer to* the tensile stress and the tensile strain, respectively.

For the study of self-recoverability, the P60-A40 hydrogel specimens were subjected to a strain of 200% under constant crosshead speed of 100 mm/min at 22 ^{o}C. After each loading, the hydrogel specimens were stored in water at 22 ^{o}C for a given time interval and then the test was repeated.

Shape memory behavior

The body temperature-responsive shape memory behavior was evaluated by a bending recovery test [33], and the detailed procedure has been provided in Scheme S1. For the photo/video demonstration of the shape memory effect, digital camera was used to record the shape fixity and shape recovery process. For a typical procedure, a hydrogel sample with given permanent shape A was initially heated by immersing in 37 ^{o}C DI water and then was deformed to a temporary shape B by applying

external force. After cooling the sample by immersing in 10 ^{o}C DI water, the sample maintained the programmed temporary shape without applying force. Subsequently, immersing in 37 ^{o}C water induced the shape recovery. Both the shape fixation and the shape recovery processes were record.

In vitro evaluation of the P60-A40 hydrogel sample using as embolization plug.

The evaluation was carried out according to previous work[18] by using a customized flow system that consisted of a peristaltic pump (Lab UIP, Kamoer) for pumping water, a heating plate (IKA, Germany) for maintaining the water at 37 ^{o}C, a 1L beaker for storing water and a measuring cylinder for calculating the flow rate. Silicone tube with an inner diameter of 2.30 mm was used to mimic arteries. DI water was used to mimic blood, and the flow rate was fixed at 120 ml/min. During the embolization, a cylinder-shaped P60-A40 specimen (2.55 mm, diameter) was initially stretched and fixed at a linear state (1.3 mm, diameter) and then was loaded into a 6-F catheter (1.4 mm, diameter). Subsequently, the linear specimen was delivered into the silicone tube though the catheter by using a guide wire under protection of 10 ^{o}C water. Because of the body temperature-responsive shape memory effect, the linear embolizaiton plug gradually recovered to its original shape, consequently, the water flow was blocked.

Additionally, dynamic mechanical analysis (DMA), Fourier-transform infrared spectroscopy (FTIR), thermogravimetric analysis (TGA), wide-angle X-ray diffraction (WAXD), scanning electron microscopy (SEM) and Cell Counting Kit-8 (CCk-8) assay were performed, respectively, to investigate the thermomechanical properties, network composition, thermal decomposition behavior,

crystalline character, micro-structure and cytocompatibility of the hydrogels, and the detailed characterization methods have been provided in the Supporting Information.

3. RESULTS AND DISSCUSION

3.1 Preparation and network structure characterizations

The chemical structure of the resulting hydrogels was confirmed by FTIR spectra (Figure S1). The band which ranges from 3035 cm^{-1} to 3063 cm^{-1} (yellow mark) is assigned to the stretching vibrations of C_{Ar}-H. [34] The peaks at 1734 cm^{-1} (green mark) and 1656 cm^{-1} (purple mark) are attributed to the stretching vibrations of C=O in PEA and amide I band, respectively. [34-35] All the absorption peaks appearing on hydrogel samples P20-A80 and P60-A40 indicate the successful introduction of PEA and AAm into one network.

The PEA moieties tend to aggregate in aqueous environment due to the strong hydrophobic association[36-37], while hydrophobic interaction is largely decreased in aprotic polar solvent DMSO [38]. Additionally, hydrogen bonding between single amide motifs have already been proven to be very weak in both water and DMSO. [16, 35] Therefore, the chemical crosslinking plays a dominant role in constructing the network of organogel. However, replacing DMSO by DI water causes the formation of hydrophobic associations between PEA moieties. Meanwhile, the aggregation of PEA moieties provides a hydrophobic micro-environment for the adjacent amide groups which further stabilize the intermolecular hydrogen bonds. [39] Owing to the formation of the dual-physical crosslinks, a contraction of hydrogel network could be clearly observed (Figure 1B). To further confirm the existence of the dual-physical crosslinks in the hydrogel network, a cylinder P60-A40 organogel

sample was cut into two halves after being fully swollen by DMSO (one half was dyed with rhodamine B for better observation), and then the two separated halves were brought into contact for several seconds using a tweezers. As expected, no connection was observed between the two halves (Figure S2 and Movie S1). However, after immersing into DI water for several seconds and subsequently bring into contact immediately with a slight force, the two havles welded rapidly to each other, and the welding zone was strong enough to withstand the weight of one half (Figure 1C and Movie S2). The observation suggests that strong physical interactions are generated across the interface and bridges the two halves as physical crosslinks when exposed to aqueous environment, implying the existence of physical crosslinks in the hydrogels.

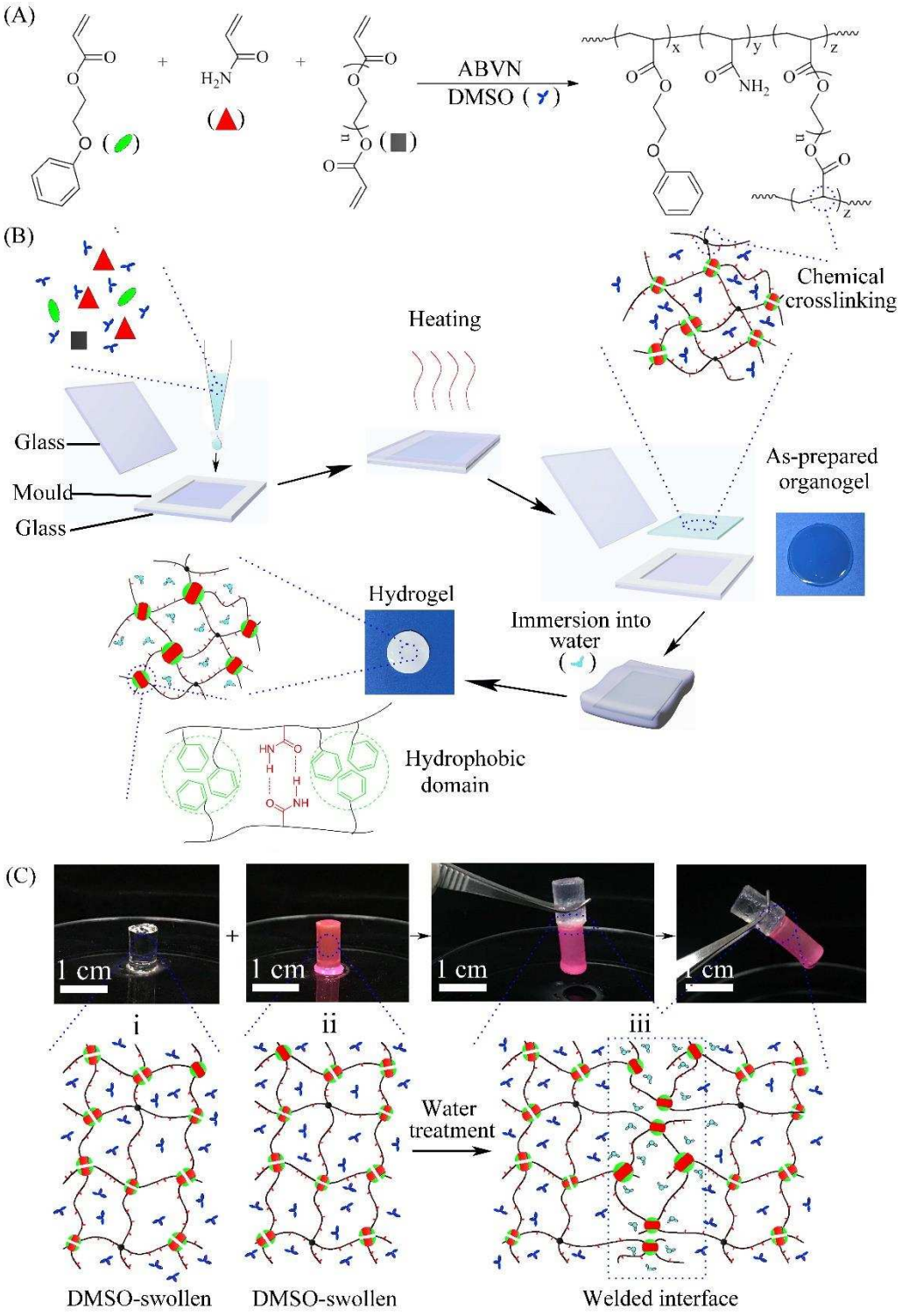

Figure 1. (A) Random co-polymerization of PEA, AAm and PEGDA700. (B) Schematic illustration of the preparation and the network architecture of poly(PEA-co-AAm) hydrogels. (C) Images

demonstrate the welding of two DMSO-swollen P60-A40 organogel networks after immersion in DI water for several seconds. The dual-physical crosslinks are dissociated in DMSO-swollen networks (i) and (ii), while partial exchange of DMSO by water at the surface causes the formation of physical crosslinks and bridging of the two networks (iii).

Further, to verify the reinforcement of amide hydrogen bonding by the hydrophobic micro-domains, reference gels were synthesized by replacing AAm with N, N- dimethylacrylamide (DMAA) to exclude intermolecular hydrogen bonds from hydrogel network. These reference gels were denoted as Px-Dy, where x and y respectively represent the percentage composition of PEA and DMAA in the total monomer. Swelling behavior tests were performed by immersing the uniform hydrogel samples P20-A80, P40-A60 and P20-D80 in 5M urea aqueous solution (a hydrogen breaking agent) [40] under 25 ^{o}C for 20 h (Figure S3). In contrast to the control samples in water, the P20-A80 gel became highly swollen in urea solution, indicating the breakage of hydrogen bonds, whereas the P40-A60 gel remained stable and no obvious change in volume was observed under the same conditions. This result suggests that the stabilization of the amide-amide hydrogen bonds becomes more striking with increasing PEA content because more micro-hydrophobic domains are formed, and thereby the amide-amide hydrogen bonds could be essentially shielded from hydrophilic environments. For the reference gel, P20-D80 remained stable throughout the swelling test, suggesting that the network expansions of P20-A80 samples were due to the dissociation of amide hydrogen bonds rather than PEA-PEA hydrophobic interactions.

After complete replacement of DMSO by DI water, the hydrogels showed a color change from light blue to white and gradually became opaque with the increase in PEA content (Figure 2A). This

phenomenon is typical in dispersion system due to the scattering of light by aggregates, suggesting the phase separation and growth of hydrophobic domains [25, 41]. Thermogravimetric analysis (TGA) curves of the hydrogels with different R_{PEA} are shown in Figure S4. The weight loss in the range of 200-250 ^{o}C was attributed to the evaporation of water associated with the polymer [42] and was progressively diminished with increasing R_{PEA}, suggesting that the hydrophobic domains prevent water molecules from associating with polymer chains. The equilibrium water contents (EWCs) of the poly(PEA-co-AAm) hydrogels with different R_{PEA} are shown in Figure 2B. Unexpectedly, the hydrogels didn't shrink monotonously when more hydrophobic PEA groups were introduced into the networks. The EWCs of the hydrogels decreased rapidly with the increase in R_{PEA} at the beginning, but showed an upward trend after R_{PEA}>40%. This abnormal swelling behavior was most likely attributed to the formation of a semipermeable layer on the surface of the hydrogel, because of the rapid phase separation during the solvent exchange in DI water. [43] As shown in Figure S5, the formation of the semipermeable structure at the hydrogel surface was clearly observed with the R_{PEA} increasing from 0 to 60 mol%. The semipermeable layer was dense enough to cause an asymmetric diffusion of water molecules during the solvent exchange, in which larger size DMSO molecules could be trapped within the polymer network while the smaller water molecules were allowed to diffuse in, until the swelling equilibrium was achieved. [43] This asymmetric diffusion caused swelling would be promoted at a higher R_{PEA}, resulting in a high EWC. Thus, the EWCs of the hydrogels were mainly determined by two factors. One is the formation of the hydrophobic micro-domains that limited the water uptake of hydrogel network. Another is the formation of the semipermeable layer that promoted the diffusion of water into hydrogel network. At low R_{PEA}, the formed semipermeable

layer was insufficient to cause an efficient asymmetric diffusion of water, because of the weak phase separation. Thus, at this stage, the swelling behavior of the hydrogels was mainly controlled by the formation of the hydrophobic micro-domains which reduced the water uptake. With the R_{PEA} increased up to 40 mol%, the formed semipermeable layer was dense enough to trap DMSO molecules effectively, resulting in an efficient asymmetric diffusion of water. This process played a dominant role in determining the swelling behavior of the hydrogels at this stage, thereby leading to an increase in EWC.

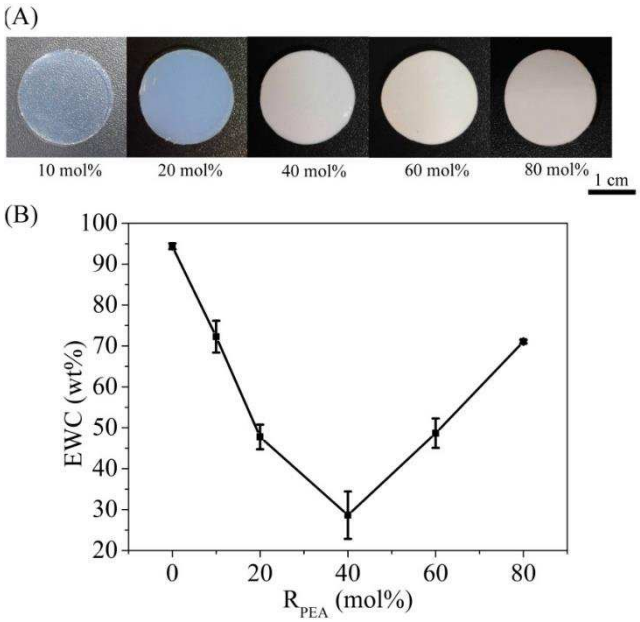

Figure 2. (A) Photographs demonstrating the poly(PEA-co-AAm) hydrogels with different $R_{PEA.}$ (B) EWCs of the poly(PEA-co-AAm) hydrogels with different R_{PEA}.

3.2 Mechanical performance

Mechanical behaviors of the organogels and the corresponding hydrogels were determined by uniaxial stretching studies. As shown in Figure 3A, the as-prepared organogels were very weak, the

tensile strength and the rupture strain of the organogels almost showed no dependence on R_{PEA}, owing to the dissociation of hydrophobic interactions and amide hydrogen bonds in DMSO. In this case, the networks were mainly constituted by covalent crosslinks, which resulted in a low crosslinking density and a lack of effective energy dissipation during deformation [44] However, after replacing and being fully swollen by DI water, the tensile strength of the corresponding hydrogels with a $R_{PEA} \geq 40$ mol% was greatly enhanced by more than one order of magnitude (Figure 3B). The formed hydrophobic interactions and the stabilized amide hydrogen bonds increase the crosslinking density and serve as sacrificial bonds to dissipate energies efficiently. The hydrogels with a $R_{PEA} \leq 20$ mol% exhibited a mechanical strength similar to that of the corresponding organogels, hinting that the formed hydrophobic interactions were weak at this level, and the hydrophobic domains were insufficient to stabilize the hydrogen bonds effectively. The difference in mechanical performance between the organogel and the hydrogel could be further identified by the area of tensile hysteresis loops which are commonly used to indicate energy dissipation capacity [45]. The tensile loading-unloading curves of both organogels and hydrogels with R_{PEA} from 20 to 60 mol% were tested, and, in contrast to the organogels, the corresponding hydrogels exhibited obvious and broad hysteresis loops on the curves (Figure S6 A, B). The dissipated energy (ΔU) at strain of 200%, which was calculated by integrating the area of hysteresis loop [46], shows a dramatic increase from organogels to hydrogels (Figure S6 C).

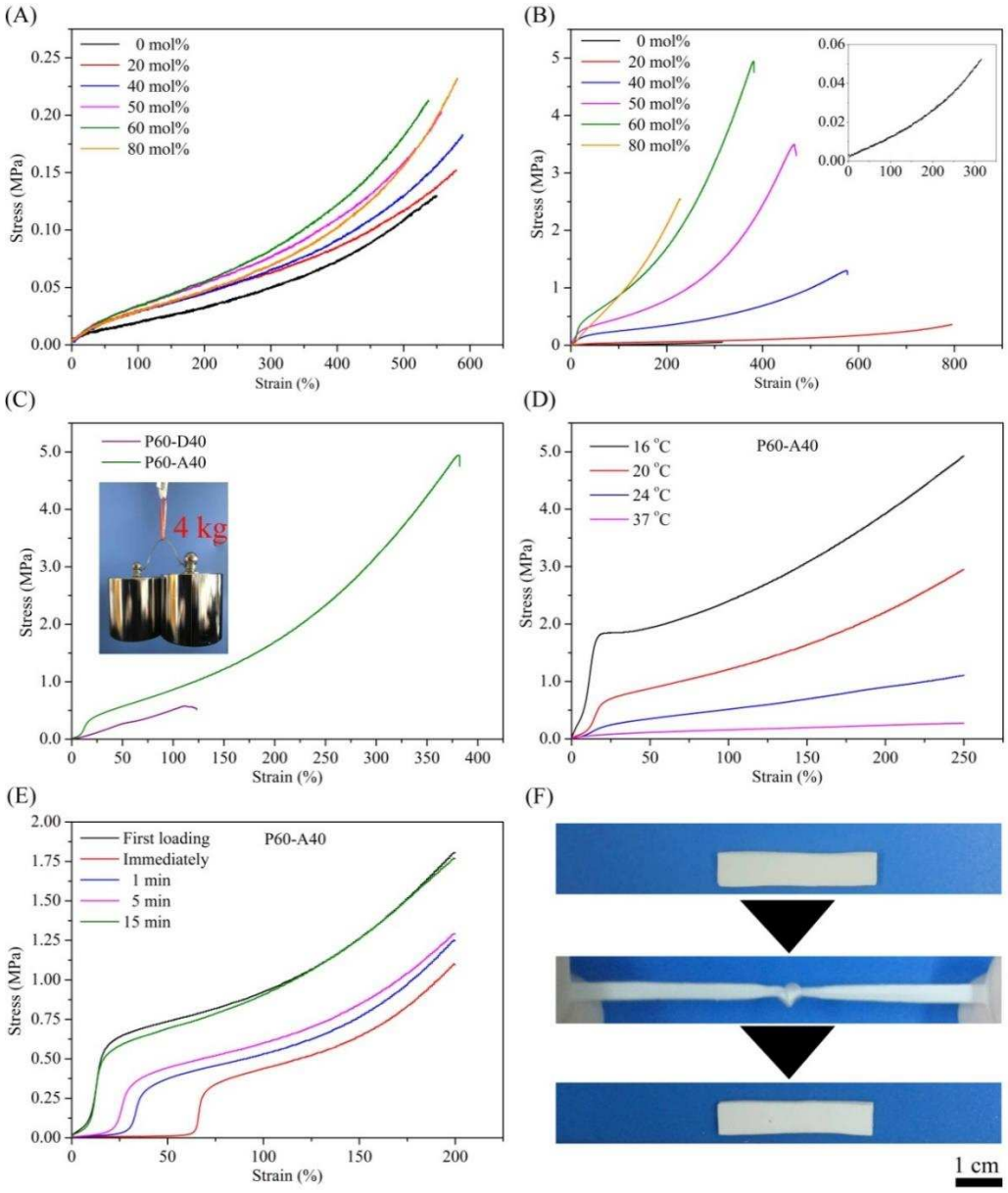

Figure 3. Mechanical performance of the as-prepared organogels and hydrogels. (A, B) The tensile stress-strain curves of the as-prepared organogels and hydrogels with different R_{PEA}. (C) The tensile stress-strain curves of the P60-A40 and P60-D40 hydrogels. Insert: a P60-A40 hydrogel sheet (size: 4.0 cm×1.0 cm×0.1 cm) lifts up 4 kg weights. (D) Uniaxial tensile behavior of the P60-A40 hydrogel under different temperature ranging from 16 to 37 ºC. The samples are not fractured at the strain of 250%. (E) Recovery of P60-A40 hydrogel samples stored in 22 ºC water for different durations. (F)

Images demonstrate the full recovery of a P60-A40 hydrogel sample (size: 3.5 cm×0.8 cm×0.1 cm) after knotting and stretching without any break.

With the increment in R_{PEA} from 0 to 80 mol%, both the rupture strain and the tensile strength first increased and then decreased, and reach the maximum value of 752.4±19.2% and 5.1±0.16 MPa at R_{PEA}=20 mol% and 60 mol%, respectively (Figure S7 A). Obviously, both of the rupture strain and tensile strength of the hydrogel P0-A100 prepared without PEA are extremely low, which is due to the lack of energy dissipation capability without the hydrophobic interactions and stabilized hydrogen bonds. However, after introducing PEA in the hydrogel networks, the mechanical performance of hydrogels are improved due to the formation of hydrophobic interactions and the enhanced hydrogen bonds. With the R_{PEA} increasing from 20 to 80 mol%, the hydrogel networks become less stretchable, which is probably due to the rigidity of the networks caused by the enhanced hydrophobic interactions.[27] The hydrogel P60-A40 exhibits the highest tensile strength, implying that the hydrophobic interactions and hydrogen bonds reach to an optimal enhancement mechanism at this point. Besides, the toughness of the hydrogels, which is calculated by extension work, reached up to 7.7±0.26 MJ/m^3 at 60 mol% of R_{PEA} (Figure S7 B). The P60-A40 hydrogel demonstrates the highest tensile strength of 5.1±0.16 MPa with a considerable rupture strain of 368.7±17.4%, and is strong enough to withstand a 4 kg weight (Figure 3C). It is obvious that the hydrogels P60-D40 and P0-A100 were much weaker than P60-A40 (Figure 3B and Figure 3C), suggesting that the mechanical performance of hydrogels where physical crosslinks only originate from either hydrophobic interactions or hydrogen bonds are inferior to that of the one with combined effect. Without the stabilization of hydrophobic domains, the hydrogen bonds of the P0-A100

hydrogel was dramatically weakened by water molecules, resulting in an extremely weak mechanical strength. The effect of the dual-physical crosslinks on the mechanical properties of our hydrogel was further investigated by testing the mechanical strength of hydrogel P20-A80 after the treatment in urea solution (Figure S8). It is clear that the hydrogel P20-A80 became much weaker after the treatment in urea solution because of the breakage of hydrogen bonds, suggesting that the stabilized amide hydrogen bonds played a significant role in dissipating deformation energy [47]. The above results suggested the positive contribution of the dual-physical crosslinks to the mechanical strength of our hydrogels.

Similar to most of the reported hydrogels that were physically crosslinked by hydrophobic interactions or hydrogen bonds[23, 25-26], the mechanical behavior of our gels also show strong dependence on temperature, which confirms the dynamic nature of the hydrophobic interactions and hydrogen bonds. As shown in Figure 3D, the P60-A40 hydrogel is weak and do not exhibit a distinct yielding at 37 ^{o}C, while decreasing temperature down to 16 ^{o}C induces a dramatic improvement in tensile strength along with a clear and higher yield point which signifies a higher energy dissipation [48]. Previous work has revealed that temperature close or above to the glass transition temperature (T_g) of the hydrophobic domains could dramatically decreased the relaxation time of hydrophobic interactions, leading to a highly frequent interdomain hopping of the hydrophobic groups, i.e., the hydrophobic interactions were highly weakened [26, 47, 49]. Since the T_g of the PEA hydrophobic domains in this work shows a value of 16.2 ^{o}C, which was determined by the T_g of poly(PEA) (PPEA, Figure S9), [26, 49] Thus, it is reasonable to believe that the temperature-dependent mechanical behavior depicted in Figure 3D is mainly attributed to the dynamic hydrogen bonds. This result

implies that although the hydrophobic interactions of PEA were weakened at this testing temperature, the hydrophobic domains still existed and stabilized the amide hydrogen bonds effectively. The dynamic property of the physical crosslinks was also confirmed by the deformation-rate dependence of tensile behavior (Figure S10). The remarkably enhanced strength of the P60-A40 hydrogel under higher deformation rate indicates a typical viscoelastic feature which is vital for energy dissipation. [50] Besides the good mechanical performance, the P60-A40 hydrogel exhibits an outstanding self-recoverability. As shown in Figure 3E, after being stretched up to a given strain of 200 %, the P60-A40 hydrogel could recover to its original state almost completely within 15 min at 22 ^{o}C without any treatment, indicating a potential fatigue resistance against repeated deformation. [40, 51] The self-recovery ability was further demonstrated by knotting and stretching, and no obvious residual strain was observed after unknotting and recovery to its original state (Figure 3F).

3.3 Dynamic mechanical analysis

Dynamic mechanical analysis was performed to gain a better understanding of the temperature-dependent mechanical behavior. As shown in Figure S11 A, the storage moduli (G') of the hydrogels vary with R_{PEA} and show a strong dependence on temperature. The hydrogels are stiff at low temperature while become soften with elevating temperature, which is attributed to the weakening or dissociation of the dual-physical crosslinking. [34] Notably, a more than 2 orders of magnitude decrease in G' was observed for P60-A40 hydrogel upon increasing the temperature from 10 to 40 ^{o}C. The plot of the loss factor (tan δ) against temperature indicates that the softening temperature of the hydrogels could be adjusted by the variation of R_{PEA} (Figure S11 B). The peak of tan δ initially migrated to high temperature and then to low temperature with the increase in R_{PEA}. The initial

migration to high temperature was likely attributed to the enhancement of the hydrophobic interactions and the stabilization of hydrogen bonds. However, the following migration to low temperature at high R_{PEA} was most probably due to a significant reduction in hydrogen bonding even though the hydrophobic interaction was further enhanced. The results suggests that the strength of the dual-physical crosslinking was varies with R_{PEA}, and the hydrogels could be adjusted to show a softening temperature below but close to 37 ^{o}C by varying monomer ratio. Obviously, the P60-A40 hydrogel shows a softening temperature of 27.6 ^{o}C, which is lower than, but close to, 37 ^{o}C, thereby could be softened easily by fingers (Figure 4A, movie S3), suggesting an excellent body-temperature sensitivity.

3.4 Body temperature-responsive shape memory behavior

Owing to the huge change of G' in response to body temperature, P60-A40 hydrogel exhibits an excellent body temperature shape memory effect. The dramatic increase in G' toward to low temperature makes the hydrogel tough enough to fix the hydrogel at any deformed state and restore the corresponding deformation energy, while, rapid decrease in G' at 37 ^{o}C induces the releasing of the deformation energy and activating the shape recovery. Figure 4B (i-iv) shows the shape recovery of a P60-A40 hydrogel sample, in which a coiled temporary shape could be fixed at 10 ^{o}C and subsequent immersion in 37 ^{o}C water activated the shape recovery. The WAXD patterns of hydrogels (Figure S12) only present broad amorphous peaks at around $2\theta=20^{o}$, indicating no crystallization domain was formed to contribute to the SME. At the molecular scale, the body temperature SME could be explained based on the reversible dual-physical crosslinks.[27,48] The association of the dual-physical crosslinks can fix the programmed temporary shapes by limiting the

mobility of the polymer chains at 10 °C, while after heating to 37 °C, the dual-physical crosslinks dissociated and the polymer chains regained their mobility, resulting in the shape recovery. The shape memory behavior of the P60-A40 was estimated quantitatively by a simple bending recovery test. [33] Results show that the shape recovery could be almost completed within 36 s (Figure S13 A), and the shape recovery process consisted of an acceleration process after a slow-down process (Figure S13 B). The acceleration process is likely attributed to the heat conduction while the slow-down process is due to the reduction of internal stress and the release of deformation energy. The hydrogel also exhibits an R_f of almost 100% (at 10 °C) and a R_r of over 95 % without obvious decrease within 4 cycles (Figure S13 C and D).

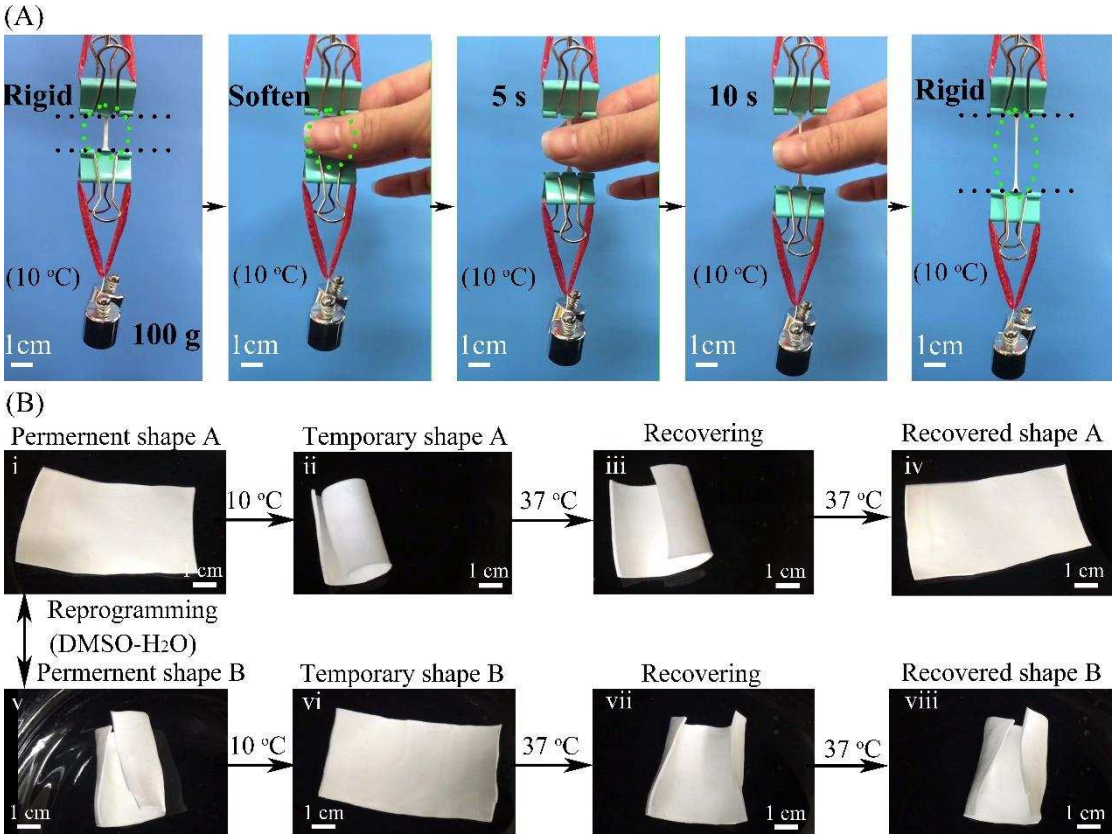

Figure 4. (A) Photo illustration of body temperature dependent mechanical strength of a P60-A40 hydrogel sheet. The sheet is rigid at a surrounding temperature of 10 °C and could bear a 100 g

weight without any obvious deformation. However, after pinching by two fingers the hydrogel becomes soft and was gradually stretched by the loaded weight. The following removal of the fingers decreases the temperature of the hydrogel and makes the hydrogel sample rigid again. (B) Images of the body temperature-responsive shape memory effect and the permanent shape reprogrammable ability. (i to iv) Temporary shape A was fixed at 10 ^{o}C, and subsequently recovered to permanent shape A at 37 ^{o}C. (v) A new coiled permanent shape B could be reprogrammed form permanent shape A after a DMSO-H_2O treatment. (vi to viii) the shape fixity and shape recovery of the new permanent shape B.

Owing to the dissociation of hydrophobic interaction and amide hydrogen bonding in DMSO and re-association in water, reprogramming permanent shape of our hydrogels could be easily realized by a sequence of DMSO-H_2O treatment (shown in Figure 4B (v-viii)). Figure S14 illustrates the detailed procedure to reprogram the new coiled permanent shape B from the permanent shape A. It is clear that the original permanent shape A was erased after the reprogramming. This reprograming process is effective for the P60-A40 hydrogel sample with any permanent shape, similarly, a sample with an as-prepared linear shape could be reprogrammed into a coiled permanent shape (Figure S15, Movie S4)

3.5 Universality of the strategy

Compared to previous works (Table S3), SMHs with body temperature responsiveness and high mechanical strength are rarely reported. How to integrate both of the element into one hydrogel network easily is still presenting challenge. The strategy used in this work shows a facile route to

highly tough SMHs with body temperature responsiveness and, to some degree, this strategy shows a possible universality. We employed other two hydrophobic monomers, benzyl acrylate (BzA) and 2-phenoxyethyl methacrylate (PEMA) to co-polymerize with AAm under the same conditions with poly(PEA-co-AAm) hydrogels to fabricate body temperature-responsive SMHs, poly(BzA-co-AAm) and poly(PEMA-co-AAm). Table S4 shows the composition, typical mechanical properties and shape memory performance of the two types of hydrogels. Results show that body temperature-responsive SME could be obtained by varying of the hydrophobic monomer content. Moreover, both of the two hydrogels exhibited considerable mechanical strength.

3.6 In vitro application as body temperature triggered embolic materials

Owing to the body temperature responsive shape memory effect, our gels show a promising application in biomedical fields, e.g., using as embolic materials in transcatheter arterial embolization (TAE) [18, 30] and noncompressible haemorrhage [52]. TAE is an effective method to treat various medical conditions such as the control of tumour and pelvic haemorrhage by embolization, while clinically used embolic materials like metal microcoils are facing drawbacks, including incomplete occlusion and repeat treatment, because of their rigid nature [30]. However, these problems could be resolved by using soft hydrogel materials. The CCK-8 assay shows that the hydrogel P60-A40 extract with the concentration as high as 20 mg/ml have no inhibition effect on 4T1 breast cancer cell viability, indicating a good cytocompatibility of the hydrogel (Figure S16). Given that the good cytocompatibility and soft nature, we tried to use the hydrogel prepared in this work as a body temperature-responsive shape memory embolization plug. The embolism performance was preliminarily explored via an in vitro measurement using a customized flow system (Figure 5A)

according to Wong et al. [18] During the measurement, a cylinder-shaped hydrogel plug (2.55 mm in diameter) was stretched into a linear shape (1.3 mm in diameter), thereby it could be loaded in a 6-F catheter (1.4 mm in inner-diameter). After delivering it into the silicon tube which is used for mimic blood vessel with a guide wire under a protection of 10 °C water, the shape recovery was triggered by blood temperature, leading to a complete block of the tube within 20 s (Figure 5B, Movie S5). Figure 5C shows that the flow rate of water was decreased monotonously and stopped within 18 s.

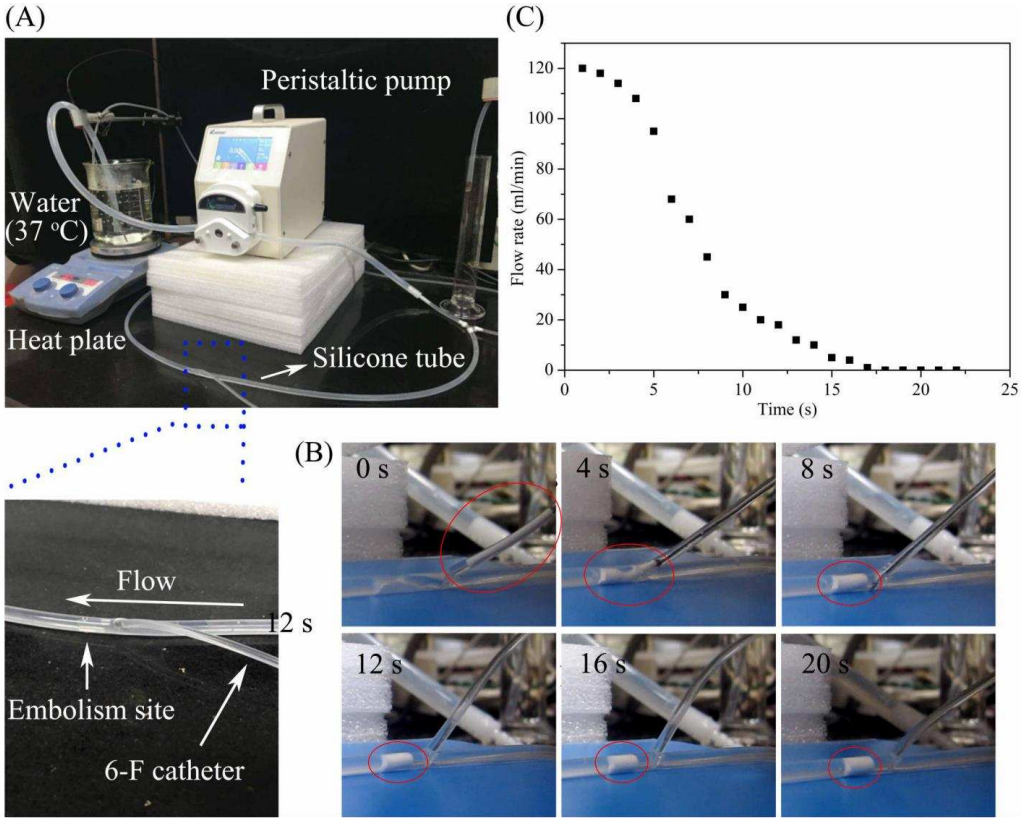

Figure 5. *In vitro* measurement of the P60-A40 hydrogel using as embolic material in TAE. (A) Image demonstrates the customized flow system consisting of a peristaltic pump, a heat plat, a 6-F catheter, a water restore and collection system, and a silicone tube network to mimic vessel. A zoomed in image demonstrating the detailed information of the embolism site and the position of the 6-F catheter. (B) Image demonstration of the embolism procedure. The shape memory embolization

plug in the red cycle gradually recover from its linear shape to the permanent cylinder shape. (C) The flow rate as a function of time.

4. CONCLUSION

In conclusion, we have successfully fabricated hydrogel networks with great mechanical strength that possess body temperature-responsive shape memory capability, resulting from synergetic dual-physical crosslinkings originating from the hydrophobic interactions and hydrogen bonds. The synergistic effect of hydrophobic interactions and hydrogen bonds result in a high toughness, fast self-recovery and considerable body temperature sensitivity. In addition, the hydrogels were applied in the application of TAE, and the embolism performance was preliminarily explored in vitro from which favorable performance was observed.

ASSOCIATED CONTENT

Supporting Information. The Supporting Information is available free of charge on the ACS Publications website at DOI:

Preparation of PPEA; Characterization methods of DMA, FTIR，TGA，WAXD；Quantitative evaluation of the shape memory performance；Cell viability assay；Swelling behavior of hydrogels in urea solution; TGA, SEM, DMA, WAXD results of hydrogels; Mechanical properties of hydrogels; Schematic illustration of the DMSO-H_2O treatment; Images of the shape fixation and

recovery of reprogrammed hydrogel P60-A40; Preparation recipes of hydrogels; Comparison of our hydrogel with previous works. (PDF)

Contact of DMSO-swollen P60-A40 samples before and after water treatment; body temperature responsiveness, shape memory effect, in vitro embolization assessment of hydrogel P60-A40 sample. (MP4)

AUTHOR INFORMATION

Corresponding Author

* Email: hjyu@zju.edu.cn (Haojie Yu)

* Email: opl_wl@dial.zju.edu.cn (Li Wang)

Notes

The authors declare no conflict of interest.

ACKNOWLEDGMENT

The authors thank Qun Pu, Li Xu and Jing He for their assistance in performing mechanical performance, DMA test and FTIR analyses, respectively, at State Key Laboratory of Chemical Engineering (Zhejiang University). The authors thank Chao Fang for his assistance in the study on cell viability assay at School of Materials Science and Engineering, Zhejiang University.

REFERENCES

(1) Löwenberg, C.; Balk, M.; Wischke, C.; Behl, M.; Lendlein, A. Shape-Memory Hydrogels: Evolution of Structural Principles to Enable Shape Switching of Hydrophilic Polymer Networks. Acc. Chem. Res. 2017, 50 (4), 723-732.

(2) Lu, W.; Le, X.; Zhang, J.; Huang, Y.; Chen, T. Supramolecular Shape Memory Hydrogels: A New Bridge between Stimuli-Responsive Polymers and Supramolecular Chemistry. Chem. Soc. Rev. 2017, 46 (5), 1284-1294.

(3) Chan, B. Q. Y.; Low, Z. W. K.; Heng, S. J. W.; Chan, S. Y.; Owh, C.; Loh, X. J. Recent Advances in Shape Memory Soft Materials for Biomedical Applications. ACS Appl. Mater. Interfaces 2016, 8 (16), 10070-10087.

(4) Zhang, Y. S.; Khademhosseini, A. Advances in Engineering Hydrogels. Science 2017, 356 (6337), eaaf3627.

(5) Guo, W.; Lu, C.; Orbach, R.; Wang, F.; Qi, X.; Cecconello, A.; Seliktar, D.; Willner, I. Ph-Stimulated DNA Hydrogels Exhibiting Shape-Memory Properties. Adv. Mater. 2015, 27 (1), 73-78.

(6) Xu, B.; Li, Y.; Gao, F.; Zhai, X.; Sun, M.; Lu, W.; Cao, Z.; Liu, W. High Strength Multifunctional Multiwalled Hydrogel Tubes: Ion-Triggered Shape Memory, Antibacterial, and Anti-Inflammatory Efficacies. ACS Appl. Mater. Interfaces 2015, 7 (30), 16865-16872.

(7) Chen, Y.; Peng, L.; Liu, T.; Wang, Y.; Shi, S.; Wang, H. Poly (Vinyl Alcohol)–Tannic Acid Hydrogels with Excellent Mechanical Properties and Shape Memory Behaviors. ACS Appl. Mater. Interfaces 2016, 8 (40), 27199-27206.

(8) Miyamae, K.; Nakahata, M.; Takashima, Y.; Harada, A. Self-Healing, Expansion-Contraction, and Shape-Memory Properties of a Preorganized Supramolecular Hydrogel through Host-Guest Interactions. Angew. Chem. Int. Ed. 2015, 54 (31), 8984-8987.

(9) Xiao, H.; Lu, W.; Le, X.; Ma, C.; Li, Z.; Zheng, J.; Zhang, J.; Huang, Y.; Chen, T. A Multi-Responsive Hydrogel with a Triple Shape Memory Effect Based on Reversible Switches. Chem. Commun. 2016, 52 (90), 13292-13295.

(10) Tang, L.; Wen, L.; Xu, S.; Pi, P.; Wen, X. Ca^{2+}, Redox, and Thermoresponsive Supramolecular Hydrogel with Programmed Quadruple Shape Memory Effect. Chem. Commun. 2018, 54 (58), 8084-8087.

(11) Le, X.; Lu, W.; Zheng, J.; Tong, D.; Zhao, N.; Ma, C.; Xiao, H.; Zhang, J.; Huang, Y.; Chen, T. Stretchable Supramolecular Hydrogels with Triple Shape Memory Effect. Chem. Sci. 2016, 7 (11), 6715-6720.

(12) Li, G.; Zhang, H.; Fortin, D.; Xia, H.; Zhao, Y. Poly (Vinyl Alcohol)–Poly (Ethylene Glycol) Double-Network Hydrogel: A General Approach to Shape Memory and Self-Healing Functionalities. Langmuir 2015, 31 (42), 11709-11716.

(13) Huang, J.; Zhao, L.; Wang, T.; Sun, W.; Tong, Z. NIR-Triggered Rapid Shape Memory Pam-Go-Gelatin Hydrogels with High Mechanical Strength. ACS Appl. Mater. Interfaces 2016, 8 (19), 12384-12392.

(14) Bilici, C.; Can, V.; Nöchel, U.; Behl, M.; Lendlein, A.; Okay, O. Melt-Processable Shape-Memory Hydrogels with Self-Healing Ability of High Mechanical Strength. Macromolecules 2016, 49 (19), 7442-7449.

(15) Zhao, Z.; Zhang, K.; Liu, Y.; Zhou, J.; Liu, M. Highly Stretchable, Shape Memory Organohydrogels Using Phase-Transition Microinclusions. Adv. Mater. 2017, 29 (33), 1701695.

(16) Zhang, Y.; Li, Y.; Liu, W. Dipole-Dipole and H-Bonding Interactions Significantly Enhance the Multifaceted Mechanical Properties of Thermoresponsive Shape Memory Hydrogels. Adv. Funct. Mater. 2015, 25 (3), 471-480.

(17) Ward Small, I.; Singhal, P.; Wilson, T. S.; Maitland, D. J. Biomedical Applications of Thermally Activated Shape Memory Polymers. J. Mater. Chem. 2010, 20 (17), 3356-3366.

(18) Wong, Y. S.; Salvekar, A. V.; Da Zhuang, K.; Liu, H.; Birch, W. R.; Tay, K. H.; Huang, W. M.; Venkatraman, S. S. Bioabsorbable Radiopaque Water-Responsive Shape Memory Embolization Plug for Temporary Vascular Occlusion. Biomaterials 2016, 102, 98-106.

(19) Park, K. H.; Kim, H.; Moon, S.; Na, K. Bone Morphogenic Protein-2 (BMP-2) Loaded Nanoparticles Mixed with Human Mesenchymal Stem Cell in Fibrin Hydrogel for Bone Tissue Engineering. J. Biosci. Bioeng. 2009, 108 (6), 530-537.

(20) Hu, X.; Zhang, D.; Sheiko, S. S. Cooling-Triggered Shapeshifting Hydrogels with Multi-Shape Memory Performance. Adv. Mater. 2018, 30 (26), 1707461.

(21) Xu, B.; Zheng, P.; Gao, F.; Wang, W.; Zhang, H.; Zhang, X.; Feng, X.; Liu, W. A Mineralized High Strength and Tough Hydrogel for Skull Bone Regeneration. Adv. Funct. Mater. 2017, 27 (4), 1604327.

(22) McDannold, N. J.; King, R. L.; Jolesz, F. A.; Hynynen, K. H. Usefulness of MR Imaging-Derived Thermometry and Dosimetry in Determining the Threshold for Tissue Damage Induced by Thermal Surgery in Rabbits. Radiology 2000, 216 (2), 517-523.

(23) Chang, X.; Geng, Y.; Cao, H.; Zhou, J.; Tian, Y.; Shan, G.; Bao, Y.; Wu, Z. L.; Pan, P. Dual-Crosslink Physical Hydrogels with High Toughness Based on Synergistic Hydrogen Bonding and Hydrophobic Interactions. Macromol. Rapid Commun. 2018, 1700806.

(24) Yang, L.; Wang, Z.; Fei, G.; Xia, H. Polydopamine Particles Reinforced Poly (Vinyl Alcohol) Hydrogel with NIR Light Triggered Shape Memory and Self-Healing Capability. Macromol. Rapid Commun. 2017, 38 (23), 1700421.

(25) Xu, C.; Tang, Q.; Yang, H. Y.; Peng, K.; Zhang, X. Y. High-Strength, Thermally Activated Shape Memory Hydrogels Based on Hydrogen Bonding between MAAc and NVP. Macromol. Chem. Phys. 2018, 219 (10), 1700636.

(26) Hao, J.; Weiss, R. Mechanically Tough, Thermally Activated Shape Memory Hydrogels. ACS Macro Lett. 2013, 2 (1), 86-89.

(27) Jiao, C.; Chen, Y.; Liu, T.; Peng, X.; Zhao, Y.; Zhang, J.; Wu, Y.; Wang, H. Rigid and Strong Thermoresponsive Shape Memory Hydrogels Transformed from Poly(Vinylpyrrolidone-*co*-Acryloxy acetophenone) Organogels. ACS Appl. Mater. Interfaces 2018, 10 (38), 32707-32716.

(28) Wang, W.; Zhang, Y.; Liu, W. Bioinspired Fabrication of High Strength Hydrogels from Non-Covalent Interactions. Prog. Polym. Sci. 2017, 71, 1-25.

(29) Argun, A.; Gulyuz, U.; Okay, O. Interfacing Soft and Hard Materials with Triple-Shape-Memory and Self-Healing Functions. Macromolecules 2018, 51 (7), 2437-2446.

(30) Zhang, Y.; Gao, H.; Wang, H.; Xu, Z.; Chen, X.; Liu, B.; Shi, Y.; Lu, Y.; Wen, L.; Li, Y. Radiopaque Highly Stiff and Tough Shape Memory Hydrogel Microcoils for Permanent Embolization of Arteries. Adv. Funct. Mater. 2018, 28 (9), 201705962.

(31) Balk, M.; Behl, M.; Nochel, U.; Lendlein, A. Shape-Memory Hydrogels with Crystallizable Oligotetrahydrofuran Side Chains. Macromolecular Symposia 2014, 345 (1), 8-13.

(32) Gao, G. R.; Du, G. L.; Sun, Y. N.; Fu, J. Self-Healable, Tough, and Ultrastretchable Nanocomposite Hydrogels Based on Reversible Polyacrylamide/Montmorillonite Adsorption. ACS Appl. Mater. Interfaces 2015, 7 (8), 5029-5037.

(33) Bai, Y.; Zhang, J.; Chen, X. A Thermal-, Water-, and Near-Infrared Light-Induced Shape Memory Composite Based on Polyvinyl Alcohol and Polyaniline Fibers. ACS Appl. Mater. Interfaces 2018, 10 (16), 14017-14025.

(34) Worzakowska, M. Starch-g-Poly(Benzyl Methacrylate) Copolymers Characterization and Thermal Properties. J. Therm. Anal. Calorim. 2016, 124 (3), 1309-1318.

(35) Dai, X.; Zhang, Y.; Gao, L.; Bai, T.; Wang, W.; Cui, Y.; Liu, W. A Mechanically Strong, Highly Stable, Thermoplastic, and Self-Healable Supramolecular Polymer Hydrogel. Adv. Mater. 2015, 27 (23), 3566-3571.

(36) Dai, Y.; Wu, F.; Li, M.; Wang, E. Properties and Influence of Hydrophobically Associating Polyacrylamide Modified with 2-Phenoxylethylacrylate. Front. Mater. Sci. Chin. 2008, 2 (1), 113-118.

(37) Gao, H. C.; Mao, S. Z.; Dai, Y. H.; Li, M. Z.; Yuan, H. Z.; Wang, E. J.; Du, Y. R. Aggregation Behavior of Acrylamide/2-Phenoxyethyl Acrylate and Its Interaction with Sodium Dodecyl Sulfate in Aqueous Solution Studied by Proton 1D and 2D NMR. Colloid. Polym. Sci. 2005, 283 (5), 496-503.

(38) Takashima, Y.; Sawa, Y.; Iwaso, K.; Nakahata, M.; Yamaguchi, H.; Harada, A. Supramolecular Materials Cross-Linked by Host-Guest Inclusion Complexes: The Effect of Side Chain Molecules on Mechanical Properties. Macromolecules 2017, 50 (8), 3254-3261.

(39) Guo, M. Y.; Pitet, L. M.; Wyss, H. M.; Vos, M.; Dankers, P. Y. W.; Meijer, E. W. Tough Stimuli-Responsive Supramolecular Hydrogels with Hydrogen-Bonding Network Junctions. J. Am. Chem. Soc. 2014, 136 (19), 6969-6977.

(40) Peng, K.; Yu, H.; Yang, H.; Hao, X.; Yasin, A.; Zhang, X. A Mechanically Robust Hydrogel with Thermally Induced Plasticity and a Shape Memory Effect. Soft matter 2017, 13 (11), 2135-2140.

(41) Chylek, P. Absorption and Scattering of Light by Small Particles. By C. F. Bohren and D. R. Huffman. Appl. Opt. 1986, 25 (18), 3166.

(42) Zhou, C. J.; Wu, Q. L. A Novel Polyacrylamide Nanocomposite Hydrogel Reinforced with Natural Chitosan Nanofibers. Colloids and Surfaces B-Biointerfaces 2011, 84 (1), 155-162.

(43) Guo, H.; Nakajima, T.; Hourdet, D.; Marcellan, A.; Creton, C.; Hong, W.; Kurokawa, T.; Gong, J. P. Hydrophobic Hydrogels with Fruit-Like Structure and Functions. Adv. Mater. 2019, 31 (25), 1900702.

(44) Zhong, M.; Liu, X. Y.; Shi, F. K.; Zhang, L. Q.; Wang, X. P.; Cheetham, A. G.; Cui, H. G.; Xie, X. M. Self-Healable, Tough and Highly Stretchable Ionic Nanocomposite Physical Hydrogels. Soft Matter 2015, 11 (21), 4235-4241.

(45) Gulyuz, U.; Okay, O. Self-Healing Poly(Acrylic Acid) Hydrogels with Shape Memory Behavior of High Mechanical Strength. Macromolecules 2014, 47 (19), 6889-6899.

(46) Gao, G.; Du, G.; Sun, Y.; Fu, J. Self-Healable, Tough, and Ultrastretchable Nanocomposite Hydrogels Based on Reversible Polyacrylamide/Montmorillonite Adsorption. ACS Appl. Mater. Interfaces 2015, 7 (8), 5029-5037.

(47) Zhang, H.; Sun, T.; Zhang, A.; Ikura, Y.; Nakajima, T.; Nonoyama, T.; Kurokawa, T.; Ito, O.; Ishitobi, H.; Gong, J. P. Tough Physical Double-Network Hydrogels Based on Amphiphilic Triblock Copolymers. Adv. Mater. 2016, 28 (24), 4884-4890.

(48) Hu, X.; Vatankhah-Varnoosfaderani, M.; Zhou, J.; Li, Q. X.; Sheiko, S. S. Weak Hydrogen Bonding Enables Hard, Strong, Tough, and Elastic Hydrogels. Adv. Mater. 2015, 27 (43), 6899-6905.

(49) Hao, J.; Weiss, R. A. Viscoelastic and Mechanical Behavior of Hydrophobically Modified Hydrogels. Macromolecules 2011, 44 (23), 9390-9398.

(50) Sun, T. L.; Kurokawa, T.; Kuroda, S.; Bin Ihsan, A.; Akasaki, T.; Sato, K.; Haque, M. A.; Nakajima, T.; Gong, J. P. Physical Hydrogels Composed of Polyampholytes Demonstrate High Toughness and Viscoelasticity. Nat. Mater. 2013, 12 (10), 932-937.

(51) Jeon, I.; Cui, J. X.; Illeperuma, W. R. K.; Aizenberg, J.; Vlassak, J. J. Extremely Stretchable and Fast Self-Healing Hydrogels. Adv. Mater. 2016, 28 (23), 4678-4683.

(52) Zhao, X.; Guo, B.; Wu, H.; Liang, Y.; Ma, P. X. Injectable Antibacterial Conductive Nanocomposite Cryogels with Rapid Shape Recovery for Noncompressible Hemorrhage and Wound Healing. Nat. Commun. 2018, 9 (1), 2784.

Table of Contents Graphic

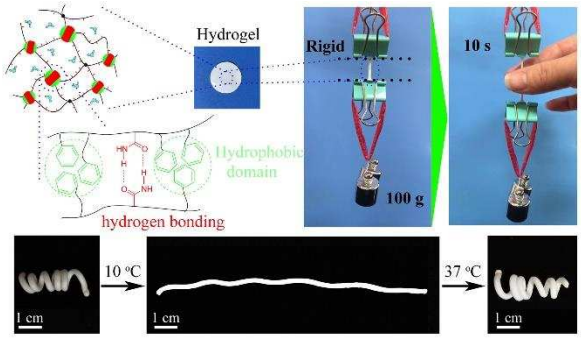

Supporting Information

Highly Tough Hydrogels with Body Temperature-Responsive Shape Memory Effect

Ruixue Liang[†], *Haojie Yu*[†,*], *Li Wang*[†,*], *Long Lin*[‡], *Nan Wang*[†], *Kaleem-ur-Rahman Naveed*[†]

[†]State Key Laboratory of Chemical Engineering, Institute of Polymer and Polymerization Engineering, College of Chemical and Biological Engineering, Zhejiang University, Hangzhou 310027, China

[‡]Department of Colour Science, University of Leeds, Woodhouse Lane, Leeds LS2 9JT,

Corresponding authors: Haojie Yu Email: hjyu@zju.edu.cn

Li Wang Email: opl_wl@dial.zju.edu.cn

Dynamic mechanical analysis (DMA)

Thermal-mechanical tests were performed on a Q800 dynamic mechanical analyzer (TA instrument, USA) under the tensile mode, fixed frequency of 1Hz, amplitude of 20 μm, heating rate of 2 ºC/min and a temperature range of 10 to 60 ºC. All the samples were cut into uniform rectangle-shaped specimens (30 mm×5 mm×1 mm) and coated with silicone grease.

Fourier-transform infrared spectroscopy (FTIR)

FTIR spectra were measured on a Nicolet 5700 spectrometer (ThermoNicolet Corporation, USA), samples were completely dried before test.

Thermogravimetric analysis (TGA)

TGA was performed on a Q500 thermo-analyzer instrument (TA, USA) from 50 to 800 ºC at a linear heating rate of 10 ºC/min under a nitrogen flow.

Wide-angle X-ray diffraction (WAXD)

WAXD measurements were performed on an X'pert powder diffractometer (PANalytical, Netherlands) with Cu-Kα radiation (λ = 0.15418 nm). Measurements were carried out in the 2θ range 5 to 80° using a step size and a step time of 0.026° and 27.54 s, respectively. Samples were completely dried before the tests.

Scanning electron microscopy (SEM)

The micro-structures of the hydrogels were determined by SEM (Zeiss, Utral 55). All the hydrogel samples were freeze-dried before the tests.

Quantitative evaluation of the shape memory performance

As shown in scheme S1 : (Step 1) A straight strip of hydrogel specimen was immersed in 37 ^{o}C DI water for 10s and then was folded into a U-shape by applying external force at the soft state. (Step 2) The folded specimen was taken out of the 37 ^{o}C DI water and immediately immersed in 10 ^{o}C DI water for 10 s to fix the temporary shape. The recovery angle and the fixed temporary angle were defined as α and 180-α, respectively. (Step 3) The bended specimen was taken out from the cold water with a tweezers and then re-immersed in the 37 ^{o}C DI water. (Step4) After re-immersing the specimen in 37 ^{o}C water, the temporary shape was recovered gradually. The recovery time and the residual angel (β) were record. The shape fixity (R_f) and shape recovery (R_r) were quantitatively determined by following equations according to Bai et al. [1]

$$R_f = \frac{180-\alpha}{180}\times 100\%, \quad R_r = \frac{180-\alpha-\beta}{180-\alpha}\times 100\%$$

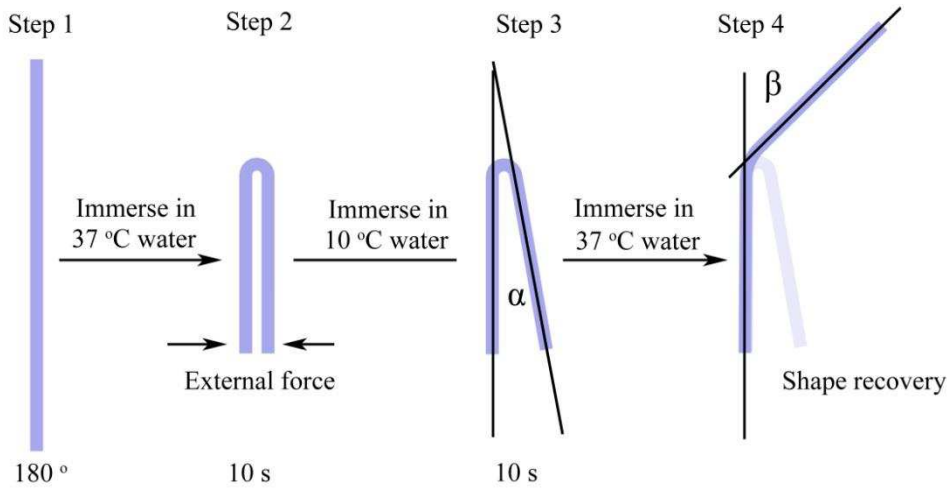

Scheme S1 Schematic illustration of the shape memory behavior test

Cell viability assay

The cytotoxicity of the hydrogel P60-A40 was assessed in vitro through a Cell Counting Kit-8 (CCK-8) assay on 4T1 breast cancer cells. 4T1 cells were seeded in 96-well plate at a density of 1.0×10^4 cells/well in 100 μl RPMI-1640 medium supplemented with 10% fetal bovine serum, 100U/ml penicillin, and 100 μg/ml streptomycin, and allowed to attach for 24h at 37 °C with 5% CO_2. The sterilized hydrogel sample was immersed in the culture medium at extraction ratios of 0, 5, 10, 15 and 20 mg/ml for 24 h at 37 °C to obtain the extracts. The culture medium in the wells was removed and replaced by the extracts. After incubation of the cells with the extracts at 37°C for 24h, CCK-8 (10 μl) was added to each well, and the cells were continuously incubated for another 1 h at 37 °C. Finally, the cell viability was determined by recording the absorbance at 450 nm using a microplate reader.

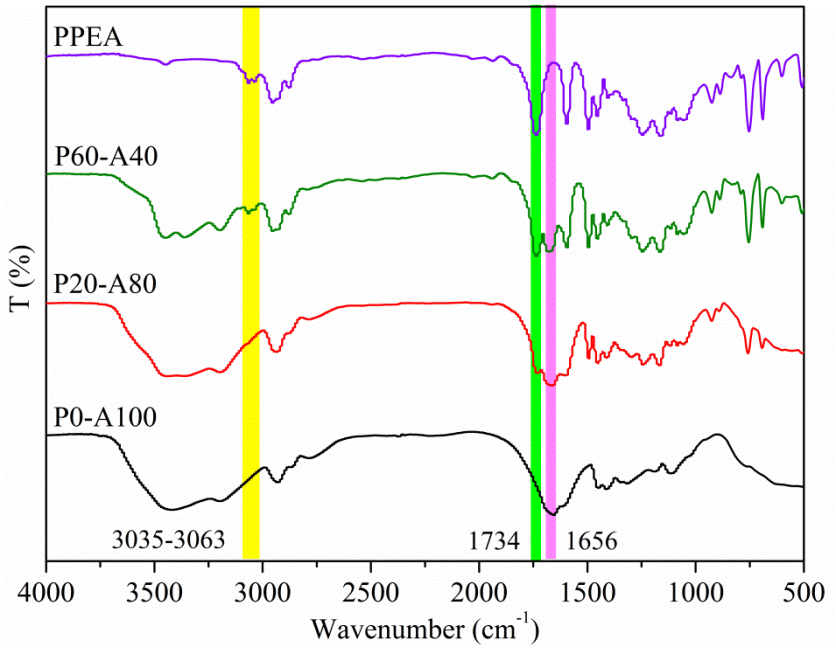

Figure S1 FTIR spectra of dried P0-A100, P20-A80, P60-A40 hydrogels and PPEA

Amide hydrogen bonds and hydrophobic interactions are dissociated in DMSO, thereby, the network of the organogel was connected only by the chemical crosslinks, PEGDA700. The photo demonstration in Figure S2 proves that no physical crosslinks formed without water treatment.

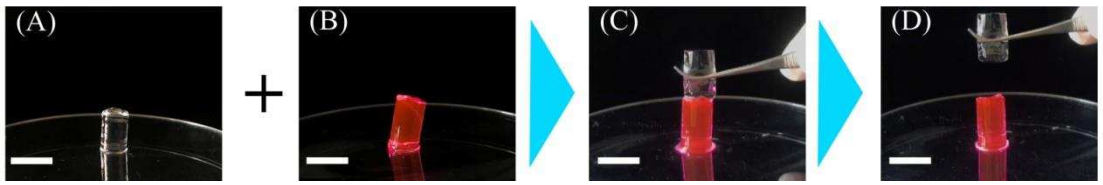

Figure S2 Images demonstrating two halves of P60-A40 organogel in (A) and (B), respectively, being brought into contact for a while at their fully DMSO swollen state, and no welding was observed. (C) Attachment of the two halves. (D) Lifting one half by a tweezers, and the two halves still remained in a separate state. The sample in (B) was dyed with rhodamine B for better observation, scale bar: 1cm.

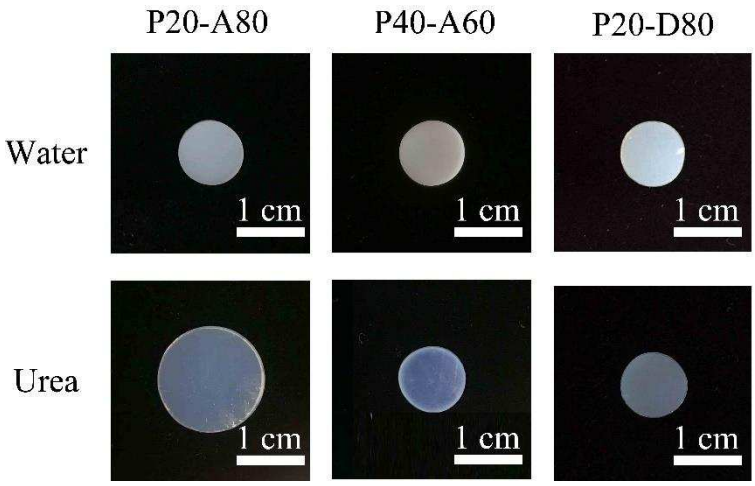

Figure S3 The swelling behavior of hydrogels P20-A80, P40-A60 and P20-D80 in water and 5M urea solution, respectively, at 25 ºC.

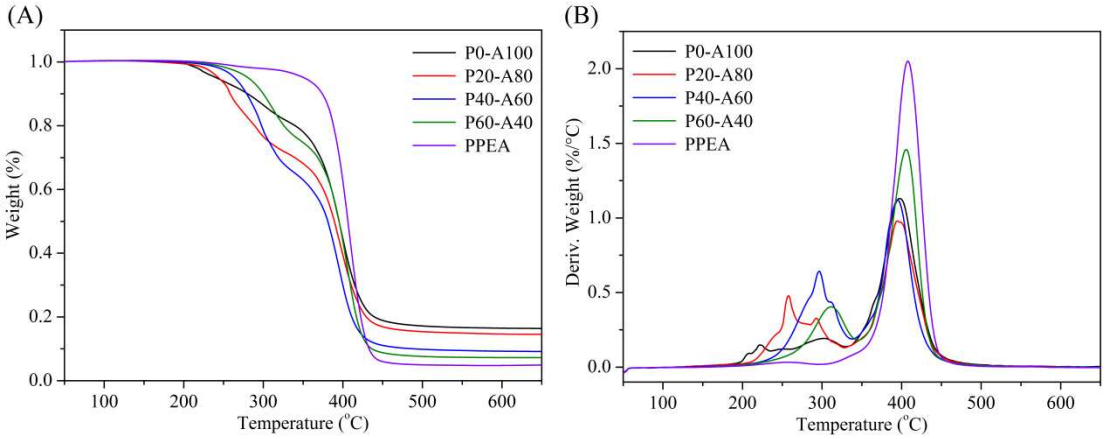

Figure S4 Thermogravimetric analysis of the dried hydrogels and PolyPEA. (A) The TG curves and (B) the corresponding DTG curves.

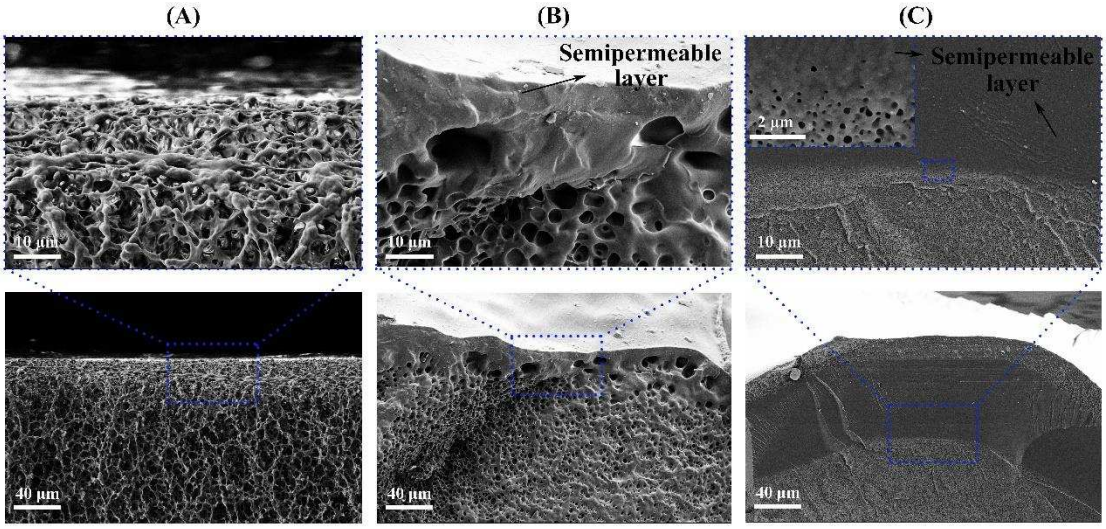

Figure S5 Microscopic structure of the cross-sections of the freeze-dried hydrogels at various magnifications. (A) P0-A100, (B) P20-A80, (C) P60-A40.

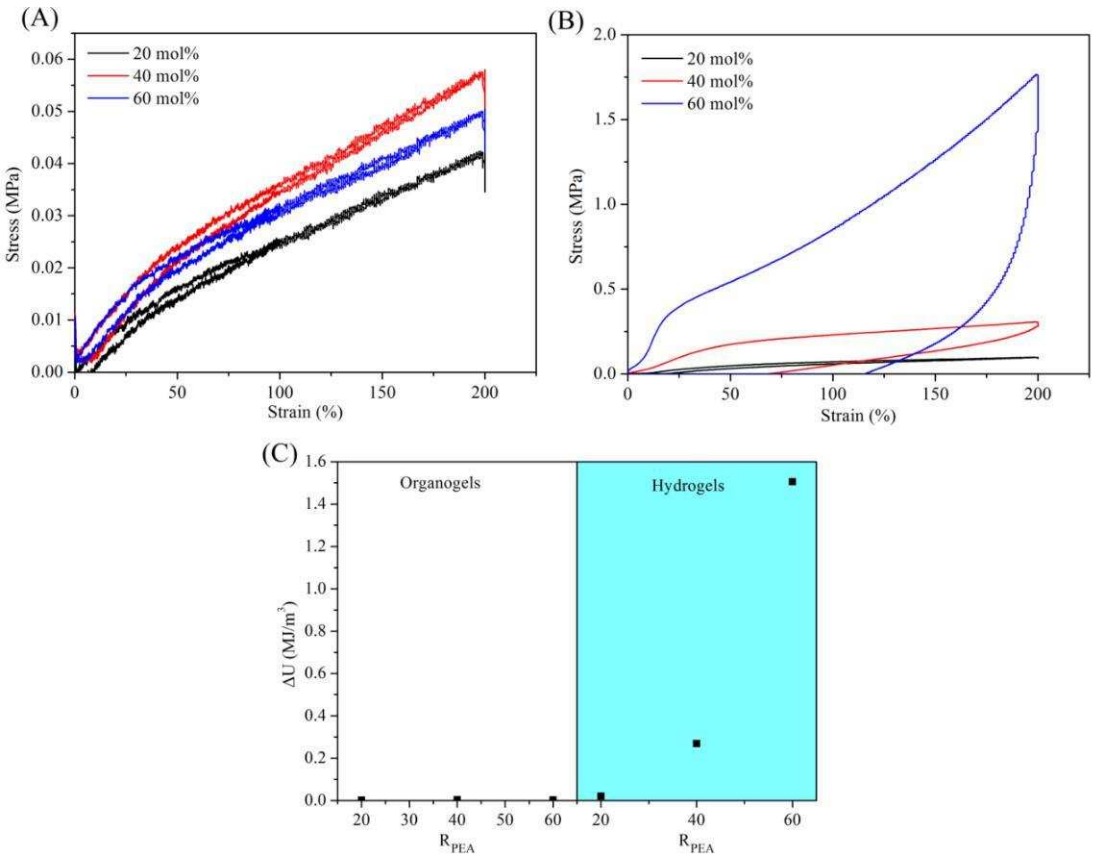

Figure S6 Samples of the (A) as-prepared organogels and (B) the corresponding hydrogels with different R_{PEA}=20, 40 and 60 were subjected to a cycle of loading and unloading to fixed strain. (C) The dissipated energy (ΔU) during the tensile loading-unloading tests of as-prepared organogels and hydrogels with strong dependence on R_{PEA}.

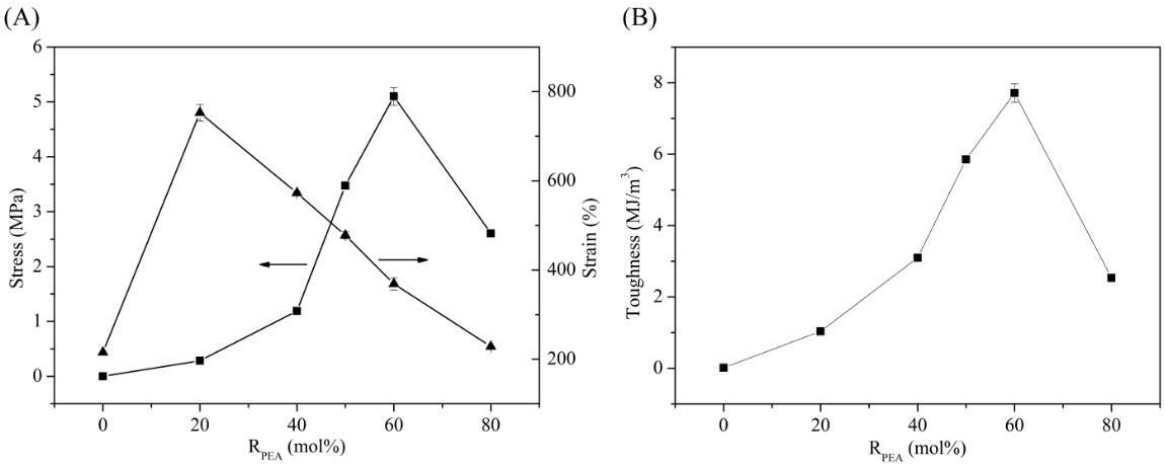

Figure S7 (A) Plotting of tensile strength, rupture strain and (B) toughness of the hydrogels against R_{PEA}

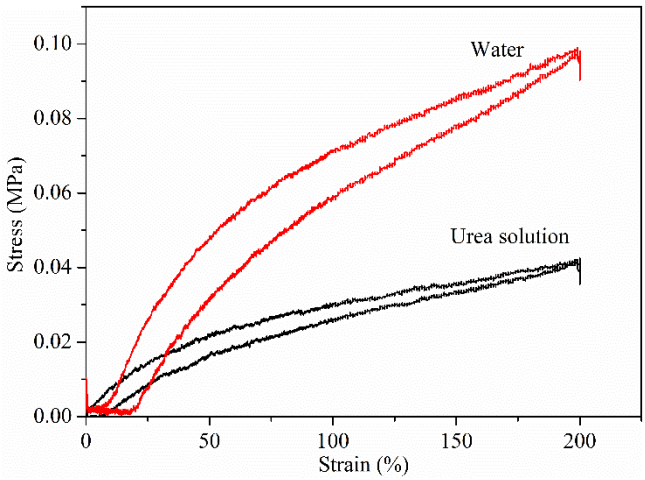

Figure S8 the loading-unloading curves of the hydrogel P20-A80 after treatment in urea solution and water, respectively.

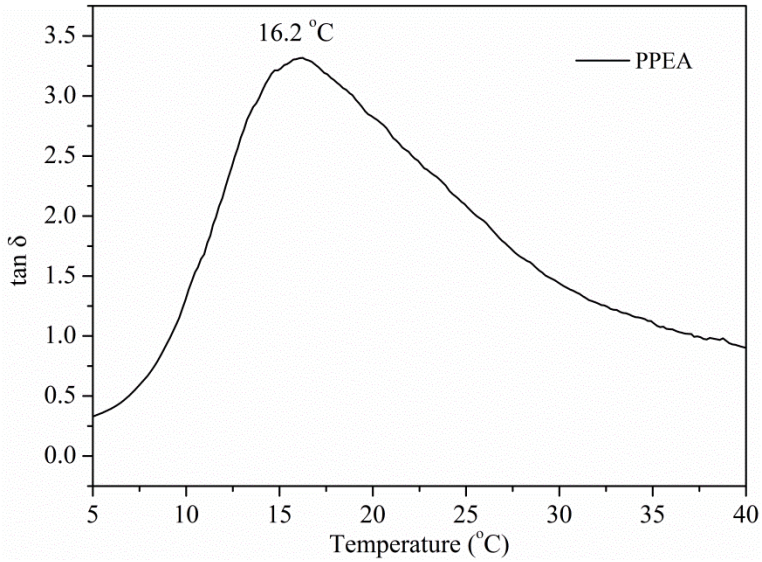

Figure S9 The loss factor (tan δ) as a function of temperature for PPEA. The peak value of 16.2 °C was used to denote the T_g of the PPEA.

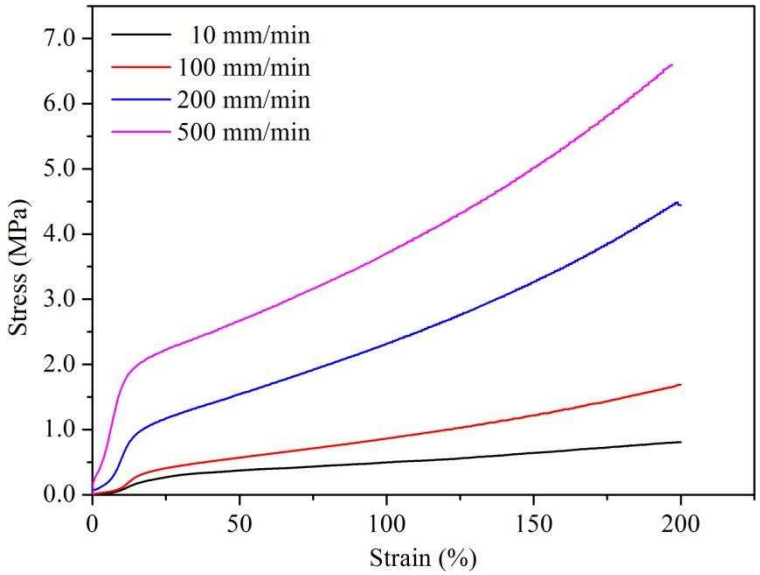

Figure S10 The deformation-rate dependence of mechanical behavior for P60-A40 hydrogel. The maximum tensile strain was fix at 200%.

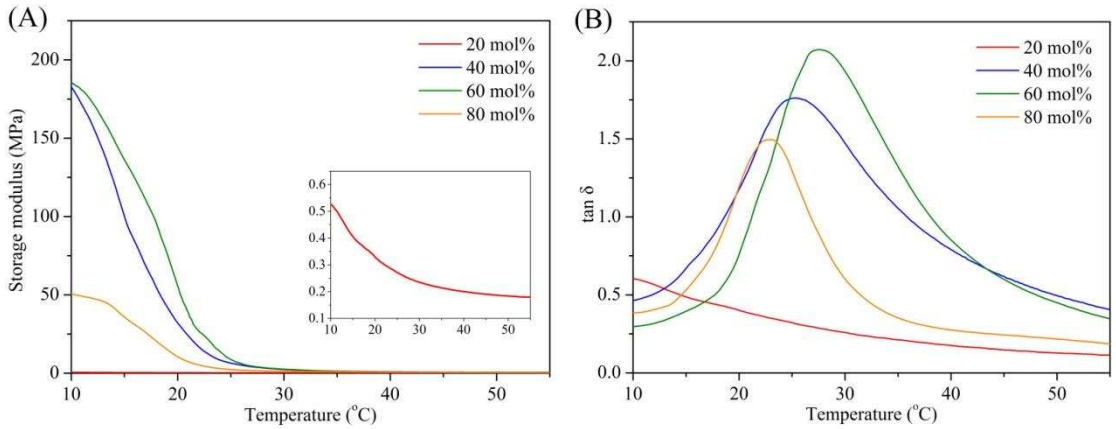

Figure S11 The (A) storage moduli and (B) loss factors (tan δ) of hydrogels with R_{PEA} ranging from 20 to 80 mol% as a function of temperature.

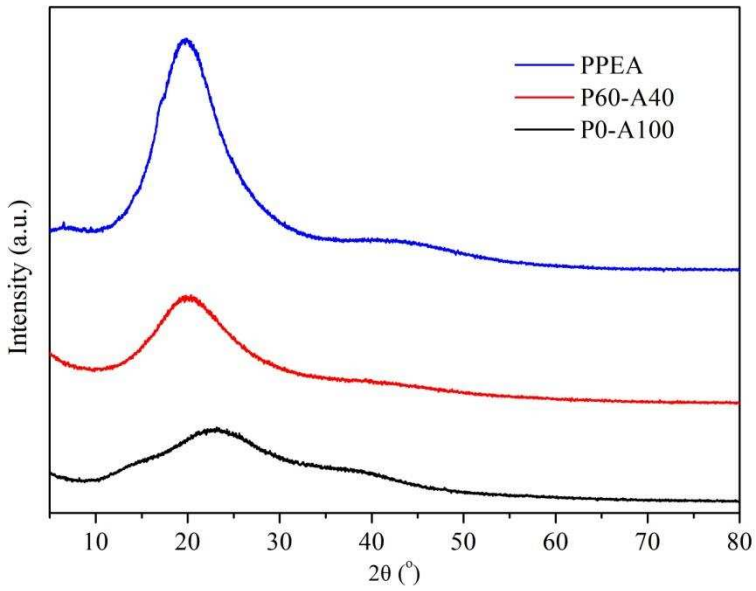

Figure S12 The WAXD patterns of the dried P0-A100, P60-A40 hydrogels and PPEA.

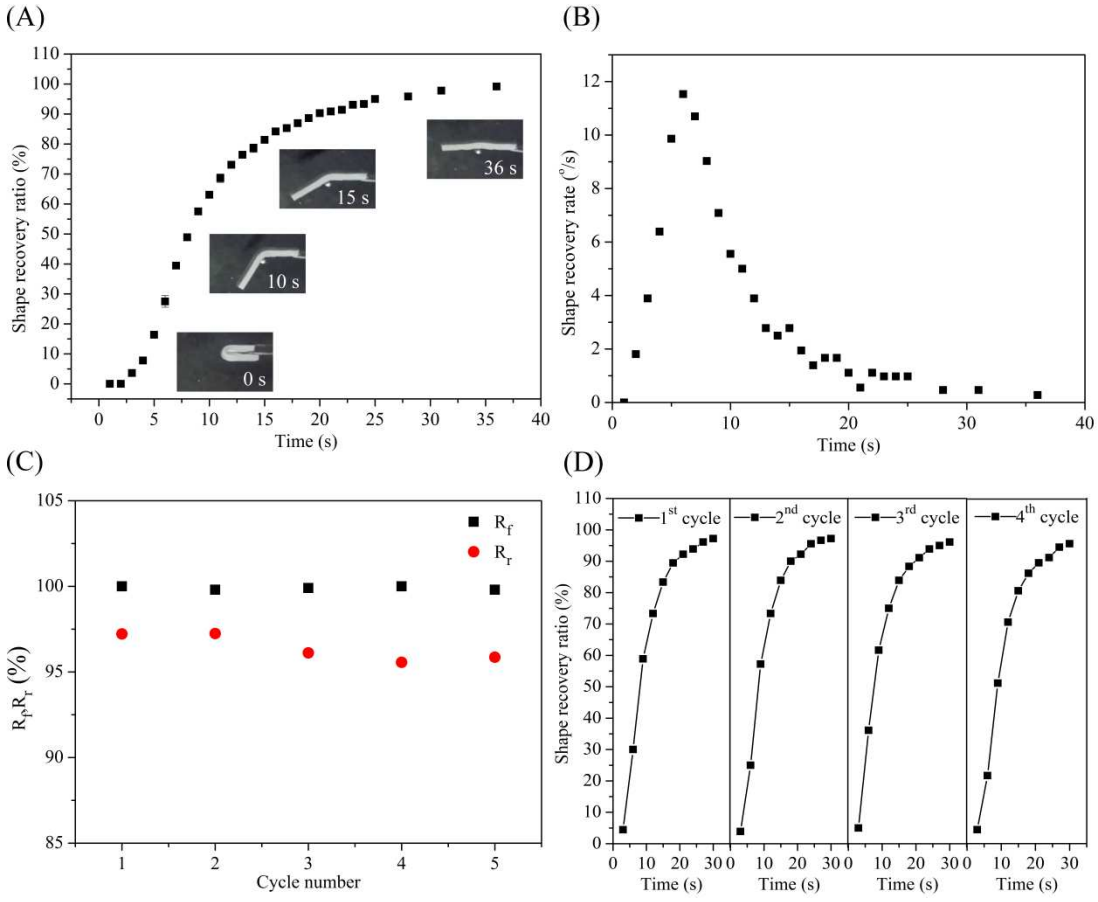

Figure S13 Quantitative evaluation of the body temperature-responsive shape memory performance of the hydrogel P60-A40. A strip-shaped hydrogel sample was fixed at a temporary U-shape through cooling (10 °C), followed by shape recovery in response to body temperature (37 °C). (A) Shape recovery process of P60-A40 hydrogel over time. (B) The shape recovery rate of P60-A40 hydrogel as a function of recovery time. (C) R_f and R_r of the hydrogel which were determinated during cyclic evaluation. (D) Cyclic shape memory behavior of the hydrogel.

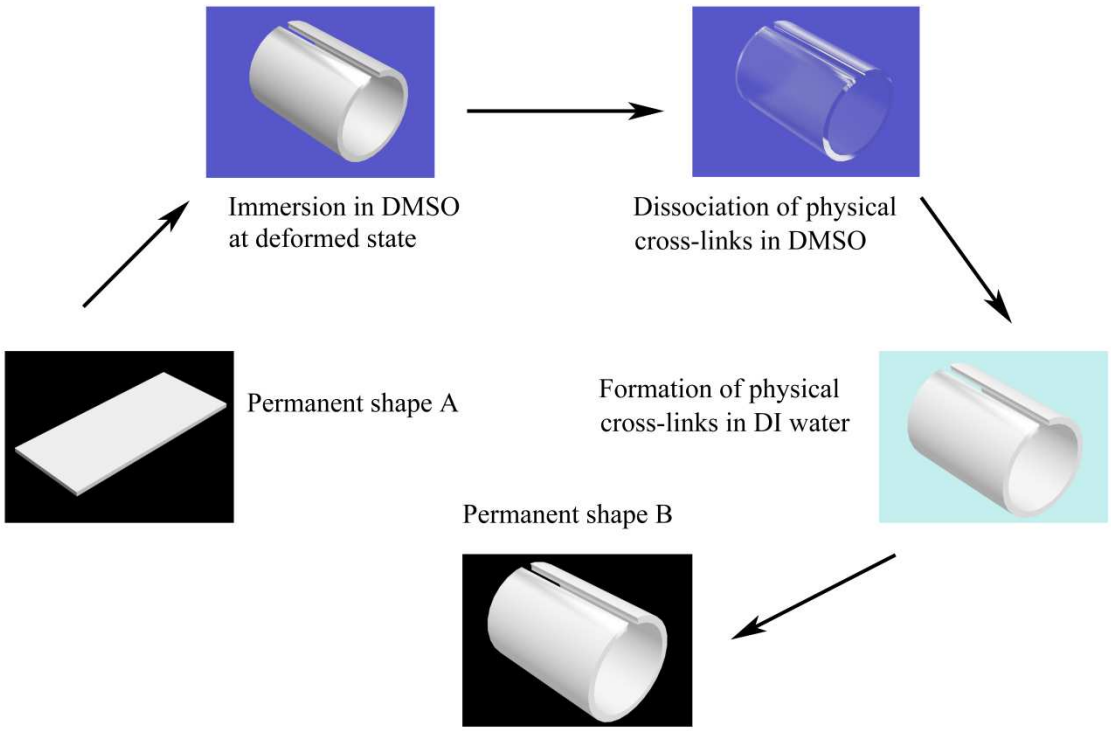

Figure S14 Schematic illustration of the permanent shape re-programming process through the DMSO-H_2O treatment.

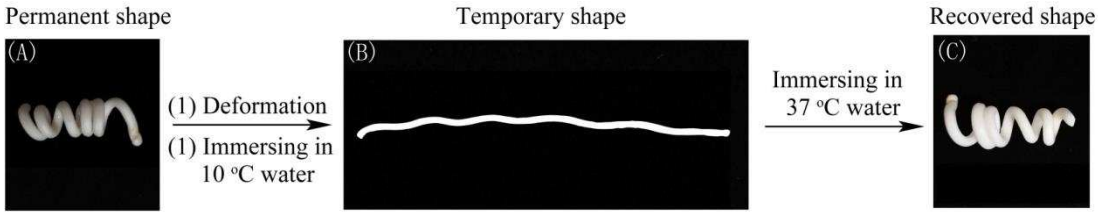

Figure S15 Shape memory behavior of the reprogrammed permanent shape (A) P60-A40 hydrogel strip with the reprogrammed coiled permanent shape; (B) the linear temporary shape was fixed by successive heating in 37 °C water, applying force and cooling in 10 °C water; (C) shape recovery of the coiled shape in 37 °C water.

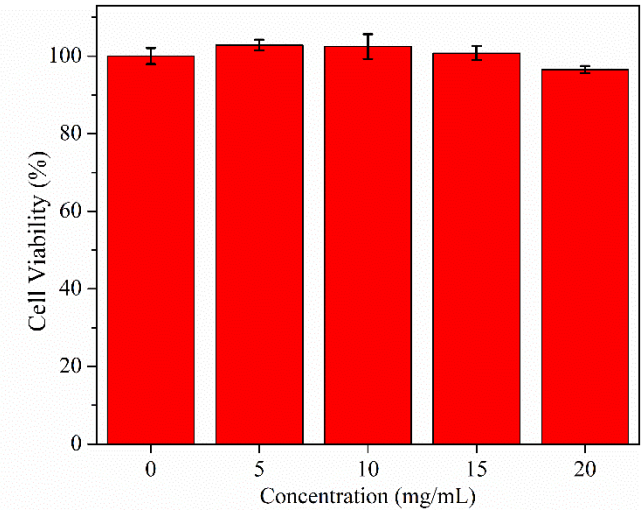

Figure S16 Cytocompatibility evaluation of the hydrogel P60-A40. All the hydrogel extracts with concentration varying from 0 to 20 presented a cell viability higher than 95%, indicating no cytotoxic content leached from the hydrogel network.

Table S1 the recipe for preparing the poly (PEA-co-AAm) and poly(PEA-co-DMAA) hydrogels

No.	PEA		AAm		DMAA		PEGDA700		DMSO	ABVN	
	mg	mmol	mg	mmol	mg	mmol	mg	mmol	ml	mg	mmol
P0-A100	0	0	4548	64.0	0	0	23.0	0.033	11.6	32.1	0.13
P10-A90	1230.1	6.4	4096.1	57.6	0	0	22.8	0.033	11.1	32.2	0.13
P20-A80	2460.6	12.8	3642.8	51.2	0	0	22.6	0.032	10.5	31.9	0.13
P40-A60	4921.9	25.6	2729.4	38.4	0	0	22.9	0.033	9.0	32.1	0.13
P50-A50	6156.5	32.0	2276.2	32.0	0	0	22.3	0.032	8.0	32.1	0.13
P60-A40	7391.0	38.5	1814.7	25.5	0	0	23.0	0.033	7.7	31.6	0.13
P80-A20	9840.0	51.2	908.1	12.8	0	0	22.8	0.033	6.5	31.5	0.13
P20-D80	1545.2	8.0	0	0	3171.1	32.0	14.2	0.02	5.0	19.6	0.08
P60-D40	4621.0	24.0	0	0	1590.3	16.0	14.1	0.02	4.5	19.5	0.08

Table S2 the recipe for preparing the poly (BzA-co-AAm) and poly(PEMA-co-AAm) hydrogels

No.	BzA		PEMA		AAm		PEGDA700		DMSO	ABVN	
	mg	mmol	mg	mmol	mg	mmol	mg	mmol	ml	mg	mmol
Poly (BzA-co-AAm)	2146.3	13.2	0	0	1364.9	19.2	11.1	0.016	5.3	15.9	0.064
Poly (PEMA-co-AAm)	0	0	1316.4	6.4	1820.6	25.6	11.3	0.016	5.3	15.8	0.064

Table S3 Parameters of typical shape memory behavior and mechanical property of thermal-responsive SMHs reported in recent years

Entry	Mechanism of shape memory effect	Trigger temperature	Tensile strength	Rapture strain	R_f	R_r	Recovery time
		^oC	MPa	%	%	%	s
Poly (PEA-co-AAm) hydrogel (this work)	association/ dissociation of hydrophobic interaction and hydrogen bonding	37	5.1±0.16	368.7±17.4	100%	>95	36
Poly(vinylpyrrolidone-co-acryloxy acetophenone) hydrogel [2]	association/ dissociation of hydrophobic interaction /π-π stacking	60-80	1.54-8.40	26	100	74-89	8-180
PVA-TA hydrogel [3]	formation/ breakage of hydrogen bonding	60	2.88-3.57	<1100	50-70	~100	5
FOSM side chain hydrogel [4]	formation/ breakage of hydrogen bonding	65	0.27−0.54	500−580	76.3-98.3	~100	N/A
Organohydrogel [5]	melting-crystallization transition	45-70	N/A	>2600	100	60-100	40
PVA-PEG double network hydrogel [6]	melting/ crystallization of crystalline microdomain	90	0.7-1.3	300-400	76-90	N/A	>15

Poly(MAAc-co-NVP-co-PEGMA) hydrogel [7]	hydrogen bonding	50	3.9	600	N/A	N/A	~30
SA-SH/PVA hydrogel [8]	melting/ crystallization of crystalline microdomain	90	N/A	N/A	40	95	120
Agarose/poly(AA-co-AAc) interpenetrating network hydrogel [9]	coil-helix transformation of agarose	70	N/A	N/A	~100	95.6	50
PAN-PAAm-PEG3kDMA hydrogel [10]	disassociation/association of dipole-dipole interaction and hydrogen bonding	37	12	~1000	97.5	100	4
Gelatin/GO/PAAm interpenetrating double network hydrogel [11]	coil-helix transition of gelatin chain	80	0.1-0.4	400-1600	0-80	N/A	N/A
DMAA-co-MAAc hydrogel [12]	formation/ breakage of hydrogen bonding	50	<2	400-850	N/A	~100	15
Physical A11AUA-based hydrophobically associated hydrogel [13]	association/ dissociation of hydrophobic interaction	60	0.017-0.89	1864-8508	N/A	N/A	~14
Biphasic Synergistic hydrogel [14]	melting-crystallization transition	40-80	0.42-0.93	100-230	100	100	N/A

Hydrogels	Hydrophobic monomer ratio	Young's modulus	Rupture strain	Tensile strength	Soften temperature	R_f at 10 °C	R_r at 37 °C	Time at 37 °C
	(mol. %)	MPa	%	MPa	°C	%	%	s
Poly (BzA-co-AAm)	40	9.01±1.38	377.2±36.8	2.36±0.14	26.69	>98.0	>98.0	30±2
Poly (PEMA-co-AAm)	20	4.38±0.45	199.9±7.3	1.98±0.02	37.45	93.3±1.7	>98.0	54±4

Table S4 The composition, mechanical properties and body temperature-responsive SME of hydrogels prepared with AAm and different hydrophobic monomers

Legends for Supplementary Movies

Movie S1：Two halves of the DMSO-swollen P60-A40 hydrogel samples were brought into contact for several seconds but no connection was observed.

Movie S2: The two halves of the DMSO-swollen P60-A40 hydrogel sample were welded rapidly after immersing into DI water for several seconds.

Movie S3: The body temperature responsiveness of the P60-A40 hydrogel.

Movie S4: The body temperature triggered shape memory performance of the P60-A40 hydrogel sample with a reprogrammed coiled permanent shape.

Movie S5: The in vitro embolization assessment of the P60-A40 sample using a customized flow system.

Reference

(1) Bai, Y. K.; Zhang, J. W.; Chen, X. A Thermal-, Water-, and near-Infrared Light-Induced Shape Memory Composite Based on Polyvinyl Alcohol and Polyaniline Fibers. ACS Appl. Mater. Interfaces **2018,** 10 (16), 14017-14025.

(2) Jiao, C.; Chen, Y.; Liu, T.; Peng, X.; Zhao, Y.; Zhang, J.; Wu, Y.; Wang, H. Rigid and Strong Thermoresponsive Shape Memory Hydrogels Transformed from Poly(Vinylpyrrolidone-Co-Acryloxy Acetophenone) Organogels. ACS Appl. Mater. Interfaces **2018,** 10 (38), 32707-32716.

(3) Chen, Y.; Peng, L.; Liu, T.; Wang, Y.; Shi, S.; Wang, H. Poly (Vinyl Alcohol)–Tannic Acid Hydrogels with Excellent Mechanical Properties and Shape Memory Behaviors. ACS Appl. Mater. Interfaces **2016,** 8 (40), 27199-27206.

(4) Hao, J.; Weiss, R. Mechanically Tough, Thermally Activated Shape Memory Hydrogels. ACS Macro Lett. **2013,** 2 (1), 86-89.

(5) Zhao, Z.; Zhang, K.; Liu, Y.; Zhou, J.; Liu, M. Highly Stretchable, Shape Memory Organohydrogels Using Phase-Transition Microinclusions. Adv. Mater. **2017,** 29 (33), 1701695.

(6) Li, G.; Zhang, H.; Fortin, D.; Xia, H.; Zhao, Y. Poly (Vinyl Alcohol)–Poly (Ethylene Glycol) Double-Network Hydrogel: A General Approach to Shape Memory and Self-Healing Functionalities. Langmuir **2015,** 31 (42), 11709-11716.

(7) Xu, C.; Tang, Q.; Yang, H. Y.; Peng, K.; Zhang, X. Y. High-Strength, Thermally Activated Shape Memory Hydrogels Based on Hydrogen Bonding between Maac and Nvp. Macromol. Chem. Phys. **2018,** 219 (10), 7.

(8) Tang, L.; Wen, L.; Xu, S.; Pi, P.; Wen, X. Ca 2+, Redox, and Thermoresponsive Supramolecular Hydrogel with Programmed Quadruple Shape Memory Effect. Chem. Commun. **2018,** 54 (58), 8084-8087.

(9) Peng, K.; Yang, K.; Fan, Y.; Yasin, A.; Hao, X.; Yang, H. Thermal/Light Dual‐Activated Shape Memory Hydrogels Composed of an Agarose/Poly (Acrylamide‐Co‐Acrylic Acid) Interpenetrating Network. Macromol. Chem. Phys. **2017,** 218 (17), 1700170.

(10) Zhang, Y.; Gao, H.; Wang, H.; Xu, Z.; Chen, X.; Liu, B.; Shi, Y.; Lu, Y.; Wen, L.; Li, Y. Radiopaque Highly Stiff and Tough Shape Memory Hydrogel Microcoils for Permanent Embolization of Arteries. Adv. Funct. Mater. **2018,** 28 (9), 201705962.

(11) Huang, J.; Zhao, L.; Wang, T.; Sun, W.; Tong, Z. Nir-Triggered Rapid Shape Memory Pam-Go-Gelatin Hydrogels with High Mechanical Strength. ACS Appl. Mater. Interfaces **2016,** 8 (19), 12384-12392.

(12) Hu, X. B.; Vatankhah-Varnoosfaderani, M.; Zhou, J.; Li, Q. X.; Sheiko, S. S. Weak Hydrogen Bonding Enables Hard, Strong, Tough, and Elastic Hydrogels. Adv. Mater. **2015,** 27 (43), 6899-+.

(13) Wei, D.; Yang, J.; Zhu, L.; Chen, F.; Tang, Z.; Qin, G.; Chen, Q. Semicrystalline Hydrophobically Associated Hydrogels with Integrated High Performances. ACS Appl. Mater. Interfaces **2018,** 10 (3), 2946-2956.

(14) Zhao, Z.; Liu, Y.; Zhang, K.; Zhuo, S.; Fang, R.; Zhang, J.; Jiang, L.; Liu, M. Biphasic Synergistic Gel Materials with Switchable Mechanics and Self‐Healing Capacity. Angew. Chem. Int. Ed. **2017,** 56 (43), 13464-13469.